LOW-COST MICROFLUIDICS ON COMMERCIAL GRADE POLY(METHYL METHACRYLATE) (PMMA) USING DEEP-UV PATTERNING

by

Marius Haiducu
M.Sc. Polytechnic Institute of Bucharest, 1986

THESIS
SUBMITTED IN PARTIAL FULFILLMENT OF
THE REQUIREMENTS FOR THE DEGREE OF

MASTER OF APPLIED SCIENCE

In the
School of Engineering Science

SIMON FRASER UNIVERSITY

Summer 2009

APPROVAL

Name: **Marius Haiducu**

Degree: **Masters of Applied Sciences**

Title of Thesis: **Low-cost Microfluidics on Commercial Grade Poly(methyl methacrylate) (PMMA) Using Deep-UV Patterning**

Examining Committee:

Chair: **Dr. Carlo Menon**
Assistant Professor
School of Engineering Science, Simon Fraser University

_____

Dr. Ash Parameswaran, Professional Engineer
Senior Supervisor
Professor,
School of Engineering Science, Simon Fraser University

_____

Dr. Albert Leung, Professional Engineer
Supervisor
Professor,
School of Engineering Science, Simon Fraser University

_____

Dr. Marinko Sarunic
Internal Examiner
Assistant Professor
School of Engineering Science, Simon Fraser University

Date Defended/Approved: July 28, 2009

Declaration of
Partial Copyright Licence

ABSTRACT

This thesis outlines a novel technique to economically pattern poly(methyl methacrilate) (PMMA) using a deep-UV radiation source in order to produce functional microfluidic components. PMMA has been used as a photoresist for many processes and applications, particularly for X-ray sources. However, the option of patterning it with inexpensive 254 nm sources has not been thoroughly explored. This thesis proposes a very inexpensive technology that can be used to pattern PMMA and produce microfluidic components. As such, this research shows that depths of well over 100 μm can be created using an un-collimated 254 nm radiation source. These depths are sufficient for creating functional microfluidic components.

Using isopropyl alcohol (IPA):water developer, we characterized the dissolution rate of commercial grade PMMA as a function of the exposure dose and etch time. This thesis also highlights the dependence of development, as well as the bonding and functional performance, of simple microfluidic units.

Keywords: poly(methyl methacrylate) (PMMA) microfluidics; deep-UV lithography; acrylic bonding

DEDICATION

To my family.

ACKNOWLEDGEMENTS

I wish to acknowledge Dr. Ash Parameswaran, my senior supervisor, for his guidance and support. To me, he has been both a mentor and a friend. As well, I am grateful to Dr. Albert Leung for being my supervisor, to Dr. Carlo Menon, and Dr. Marinko Sarunic for accepting to be part of my thesis committee.

Warm thanks go out to my colleagues in the lab, Robert Johnstone, Dan Sameoto, Ian Foulds, Manu Venkataram, Mona Rahbar, Sae-Won Lee, and Ajit Khosla for their assistance and support. Within the School of Engineering Science, I would like to thank Mr. Steve Whitmore and Mr. Mike Sjoerdsma for reading my thesis. Thanks also go out Bill Woods for his valuable feedback on my cleanroom work and to Dr. Bonnie Gray for allowing me to use the syringe pump to perform the leakage tests.

Finally, I would like to thank my family – my wife and my son – without whom my life as a student would have been more difficult.

TABLE OF CONTENTS

Approval ..... **ii**

Abstract ..... **iii**

Dedication ..... **iv**

Acknowledgements ..... **v**

List of Figures ..... **viii**

List of Tables ..... **x**

LIST OF ABBREVIATIONS ..... **xi**

1 Introduction **1**

1.1 Objectives 2
1.2 Chapter Outline 4

2 PMMA as a Structural Material for Microfluidic Applications **5**

2.1 Early Microfluidic Materials and Processes 6
2.2 Polymer or Plastic Microfluidics 7
2.3 PMMA Microfluidics 10
2.4 PMMA Patterning Through Exposure and Development 13
2.4.1 Exposure of PMMA 14
2.4.2 Development of PMMA 17

3 Process Development **21**

3.1 Irradiation Source 21
3.2 Substrates 22
3.2.1 Optical Absorbance 23
3.3 Process Steps 27
3.3.1 PMMA Patterning 27
3.3.2 Microfluidic Device Fabrication 32

4 Process Characterization **34**

4.1 Dissolution Rates 34
4.2 Effect of a Titanium Barrier Layer 37
4.3 Effect of Temperature and Agitation 39
4.4 Considerations on Aspect Ratio and Side Walls 42
4.5 Test of Microfluidic Channels 44

5 Process Improvements **47**

5.1 In-house Built Irradiation Source 48

5.2 Light Semi-collimation 51
5.3 Adhesion/Bonding of Microfluidic Devices 53

6 Summary 56

6.1 Future Work 56
6.2 Conclusions 58

Appendices 59

Appendix A: Letter from Dr. Ian Forbes, publisher with the Journal of Micromechanics and Microengineering 60
Appendix B: OPTIX® and GoodFellow CQ Grade Acrylic Sheet Properties 61
Appendix C: Acrylite® OP-4 Acrylic Sheet Properties 62
Appendix D: Absorption Measurements for UVT OP-4, OPTIX®, and PMMA 495kDa 63
Appendix E: PMMA Patterning Process Recipe 64
Appendix F: Etch Depths of OPTIX® PMMA Exposed with Multiple Doses of 216 J/cm^2 of Deep-UV Radiation 65
Appendix G: Etch Depths of UVT OP-4 PMMA Exposed with Multiple Doses of 216 J/cm^2 of Deep-UV Radiation 66
Appendix H: Etch Depths of OPTIX® PMMA Exposed Through a 5 nm Thick Titanium Barrier Layer with Multiple Doses of 216 J/cm^2 of Deep-UV Radiation 67
Appendix I: Etch Depths of OPTIX® PMMA Exposed with Multiple Doses of 216 J/cm^2 of Deep-UV Radiation. Development Performed With Mechanical Agitation 68
Appendix J: Etch Depths of UVT OP-4 PMMA Exposed with Multiple Doses of 216 J/cm^2 of Deep-UV Radiation. Development Performed With Mechanical Agitation 69
Appendix K: Sequence of Pictures Taken During the Microfluidic System Test 70
Appendix L: Power Supply and Control Circuit - Schematic Diagram 71
Appendix M: Photodiode GUVB-T11GD Data Sheet 72
Appendix N: Electronic Circuit Used to Measure the Deep-UV Power Levels Inside Stratalinker 2400 and the In-house Built Irradiation Box 73
Reference List 74

LIST OF FIGURES

Figure 2-1: Fragmented molecular weight vs. density of main chain scissions. Initial number average molecular weights of 60 (OPTIX®), 300 (UVT), and 600 (CQ Grade) kDa were chosen for representation (adapted from [90]). 15

Figure 3-1: Absorbance of three different types of acrylic versus exposure time. Each 5 hours of exposure correspond to a dose of 72 J/cm^2. 25

Figure 3-2: Deep-UV exposure of PMMA: process steps. 27

Figure 3-3: Photograph of a PMMA sample on which the gold hard mask was sputtered and patterned. 29

Figure 3-4: Photograph of Stratalinker 2400 used as a deep-UV radiation source. 30

Figure 3-5: Development setup consisting of a bath - whose temperature is monitored by a thermocouple – on top of a programmable hotplate 31

Figure 4-1: Etch depth versus time for OPTIX® PMMA exposed with multiple doses of 216 J/cm^2 of deep-UV 35

Figure 4-2: Etch depth versus time for UVT OP-4 PMMA exposed with multiple doses of 216 J/cm^2 of deep-UV 35

Figure 4-3: Etch depths versus time for OPTIX® PMMA exposed through a 5nm thick Ti barrier layer with multiple doses of 216 J/cm^2 of deep-UV. 38

Figure 4-4: Profilometry measurements of developed PMMA after a 1080 J/cm^2 dose followed by 40 min (left) and 60 min (right) of development, respectively. 39

Figure 4-5: Developer bath setup when agitation is introduced during development. 40

Figure 4-6: Etch depths versus time for OPTIX® PMMA exposed with multiple doses of 216 J/cm^2 of deep-UV. Development was performed with mechanical agitation. 41

Figure 4-7: Etch depths versus time for UVT OP-4 PMMA exposed with multiple doses of 216 J/cm^2 of deep-UV. Development was performed with mechanical agitation. 41

Figure 4-8: SEM images of patterned CQ PMMA after 10 min of development a) and b) and 50 min of development c) and d). Small features are completely undercut due to negative side walls. 43
Figure 4-9: Fully assembled system under test. 44
Figure 4-10: Close-up of the microfluidic chip under test with inset of tube attachment..... 45
Figure 4-11: A “Y” channel under test (left) and a close-up of the liquid flow (right)..... 46
Figure 5-1: The in-house built irradiation box: front view. 49
Figure 5-2: The in-house built irradiation box: rear view..... 49
Figure 5-3: The new irradiation box with the rotational stage. 52
Figure 5-4: The new irradiation box with the rotational stage over which a plastic grate was set in order to semi-collimate the light..... 52
Figure 5-5: Microfluidic chip bonded using an intermediary layer of 950 kDa PMMA. 55
Figure K-1: Snap shots showing the laminar flow of the red and blue colored water through the microchannels. A “Y”- channel is shown on the left and a channel cross on the right. 70
Figure L-1: Schematic diagram of the power supply and the control circuit for the germicidal lamps ballasts. 71
Figure M-1: Responsivity curve of GUVB-T11GD. 72
Figure N-1: Schematic diagram of the electronic circuit used to measure the deep-UV power levels. 73

LIST OF TABLES

Table 2-1: Materials of construction for electrokinetic microfluidic devices reproduced from [37]. 9

Table 2-2: Properties of different polymers. The data was compiled from [64]. 11

Table B-1: OPTIX® acrylic sheet properties [140]. 61

Table B-2: GoodFellow CQ grade acrylic sheet properties [143]. 61

Table C-1: Acrylite® OP-4 acrylic sheet properties [144]. 62

Table D-1: Direct (i.e., not normalized for thickness) absorption readings 63

Table D-2: Absolute absorbance values for UVT OP-4, OPTIX®, and PMMA 495 kDa. 63

Table E-1: PMMA patterning process recipe. 64

Table F-1: Etch depths of OPTIX® PMMA (development without agitation). 65

Table G-1: Etch depths of UVT OP-4 PMMA (development without agitation). 66

Table H-1: Etch depths of OPTIX® PMMA exposed through a 5 nm thick Ti barrier layer. 67

Table I-1: Etch depths of OPTIX® PMMA (development with agitation). 68

Table J-1: Etch depths of UVT OP-4 PMMA (development with agitation). 69

Table M-1: Absolute maximum ratings for GUVB-T11GD. 72

Table M-2: Characteristics of GUVB-T11GD (at 25°C). 72

LIST OF ABBREVIATIONS

The following is a list of acronyms that are referred to in this thesis:

CQ	Clinical Quality
DC	Direct Current
DI	De-Ionized
DRR	Dissolution Rate Ratio
EOF	Electroosmotic Flow
GPC	Gel Permeation Chromatography
IPA	Isopropyl Alcohol
LIGA	Lithographie Galvanoformung Abformung
MEK	Methyl Ethyl Ketone
MIBK	Methyl Isobutyl Ketone
PC	Polycarbonate
PDMS	Poly(dimethylsiloxane)
PETE	Poly(ethylene terephtalate)
PGMEA	Propylene Glycol Methyl Ether Acetate

PMGI	Poly(methylglutarimide)
PMMA	Poly(methyl methacrylate)
PPy	Polypyrrole
PR	Photoresist
PTFE	Poly(polytetrafluoroethylene)
SEM	Scanning Electron Microscope
THF	Tetrahydrofuran

1 INTRODUCTION

A key role in science, especially in fields such as drug discovery, pharmaceutical screening, medical diagnostics, DNA analysis, environmental analysis, etc., is played by the precise and thorough determination of chemical or biological parameters of a certain substance, cell, or tissue [1-7]. More often than not, the analyte of interest comes in small quantities, or it is quantitatively negligible with respect to the mass of substance in which it resides. As such, for the sake of efficiency, analyte detection and separation calls for the miniaturization of the scale at which the analysis is performed. A miniaturized analysis system brings about better process control and throughput, an increased response time, superior analytical performance, a steep decrease in the analyte waste, lower power consumption, and lower heat generation. Portability and disposability can be added to the long list of advantages as well. Additionally, a micro or nanometre-sized system facilitates the investigation of either fluid transport or molecular behaviour at very small dimensions [8, 9].

The transition from macro to micro and nano-scale has been facilitated by the manufacturing methods used in the microelectronics industry for more than five decades. Accordingly, silicon and silicon-compatible materials started to be used for creating microchannels and micro-reservoirs, which represented the

core of any miniaturized chemical or biological system. However, the high manufacturing costs [10], the low fabrication turn-around, and the incompatibility of silicon and glassy materials with certain chemical and biological reagents [11] shifted interest toward developing microfluidic chips in polymers and plastics [12].

Currently, polymers and plastics are used overwhelmingly as substrate materials for microfluidic devices. Nevertheless, the most productive manufacturing methods, such as mass replication (e.g., hot embossing or injection moulding) or rapid prototyping (e.g., laser micromachining or casting) technologies require the use of either a master, which is usually expensive to produce, or pricey equipment. By proposing a novel method of patterning microfluidic channels in inexpensive commercial acrylic substrates, using a reasonably priced exposure system and relatively non-toxic materials, our work offers a viable and economical alternative to the production systems in existence today.

1.1 Objectives

The main objective of this work is to characterize the patterning of commercial poly(methyl methacrylate) (PMMA) using a light source with a wavelength of 254 nm. Exposure of PMMA with this particular wavelength has not been well addressed in the literature because exposure with 240 nm was considered the upper limit of the effectiveness [13]. Only relatively recently has this wavelength been used to irradiate thin layers of spin-coated PMMA [14, 15]. As a result, the research community has recognized the novelty of our work by

selecting our paper [16] to be part of the *Journal of Micromechanics and Microengineering (JMM) Highlights of 2008*. A copy of the announcement letter addressed to us by the publisher of JMM is shown in Appendix A.

PMMA has been used for decades as a positive resist for advanced radiation microlithography [17]. The radiation sensitivity of PMMA translates into main polymer chain scissions inflicted by the absorbed radiation. Backbone cleavages lower the average molecular weight of PMMA and that, in turn, brings about increased solubility. This approach is, otherwise, the general photolithographic method of transferring a latent image in the resist into a physical pattern.

In this thesis, the 254 nm radiation was performed using a Stratalinker 2400, manufactured by Stratagene[1], which is equipped with low-pressure mercury-vapour lamps [18]. Although the radiation intensity is fairly low (only 4mW/cm^2) and the light is not collimated, Stratalinker is inexpensive – at least compared with gamma rays, X-rays, e-beam, proton beam, or ion beam sources used traditionally for patterning PMMA. This simple unit is capable of exposing an area of 1,567 cm^2.

A second objective of this thesis is the fabrication and testing of a microfluidic device consisting of an array of channels and reservoirs. This testing was performed by sealing the patterned channels with a blank piece of PMMA, drilling access holes into the reservoirs, attaching poly(tetrafluoroethylene)

[1] Stratagene is an Agilent Technologies Division.

(PTFE) tubing to the chip, and running a dyed fluid at different flow rates through microchannels.

A third and final objective is the identification of modalities to improve the overall process. This objective was accomplished by increasing the radiation power and its collimation, introducing a new developer, and finding novel bonding methods.

1.2 Chapter Outline

The main work presented in this thesis involved using commercial grade PMMA as the structural material for creating low-cost microfuidic devices. Chapter 2 offers background information about the materials and processes used for creating microfluidic devices, discussing polymers and plastics in general, and PMMA in particular. This explanation is followed by a discussion on the exposure and development of PMMA using different sources and solvents. Chapter 3 outlines the process development. The process characterization is covered in chapter 4. Chapter 5 addresses aspects related to the process improvement and the final chapter provides overall conclusions regarding the findings in this thesis.

2 PMMA AS A STRUCTURAL MATERIAL FOR MICROFLUIDIC APPLICATIONS

Microfluidics, a modern interdisciplinary science positioned at the confluence of chemistry, physics, biology, and engineering, studies the behaviour of fluids at the micro and nano-scales, as well as the design of the systems that are able to handle such tiny volumes of fluid [7]. Undoubtedly, the most-used device in microfluidics is the microchannel, with different geometric designs. Historically, glass and silicon have been the preferred materials for fabricating microchannels because fabrication methods were already established by the semiconductor industry [12]. Gradually, those traditional substrates are being replaced by plastic to reduce costs and simplify fabrication procedures. Furthermore, plastics with a wide variety of material properties and prefabricated shapes are available, offering the flexibility to produce rapidly samples and devices for targeted applications.

A quick survey of the materials as well as the fabrication methods used for microfluidic applications are the focus of the first part of this chapter. A rationale of why PMMA and deep-UV were the substrate and, respectively, the irradiation source of choice for the work herein follows.

2.1 Early Microfluidic Materials and Processes

Silicon, quartz, glass, and even metals were the first materials used for creating microchannels and microfluidic devices, employing techniques borrowed from the microelectronics industry. Glass and silicon microfluidic chips were first developed by Manz and co-workers [19], who coined the concept of micro-total-analysis-system (μTAS) – a system designed to handle the total sequence of lab processes aimed to perform one or more chemical analysis. In a μTAS , a user would introduce the sample and the device would perform the entire testing protocol comprised of sample preparation, separation, and detection [20, 21]. Later on, the superiority in terms of analytical performance, through minimization of the scale at which the analysis is carried out, has been demonstrated experimentally and theoretically [19, 20].

Eventually, a new miniaturization-related term was introduced: lab-on-a-chip (LOC), which indicated the scaling of laboratory processes down to a chip format. In 1975, S.C. Terry developed a gas chromatograph [22] on silicon, which was the first LOC. Currently, LOC technologies and devices are employed in a wealth of application areas, such as separation science, protein analysis, process control, chemical synthesis, immunoassays, cell manipulation, and DNA sequencing and amplification [4].

The photolithographic techniques are the most popular for creating microchannels in the aforementioned materials [23-32] . Further, for silicon, bulk [33] or surface micromachining [34] can be used to create microchannels [35].

Separation methods, specifically electrophoretic separation [20, 36], were the focus of the early microfluidics work using the aforementioned materials. However, capillary electrophoresis (CE) chips fabricated in silicon, although reported [37, 38], encountered conductivity problems when high voltages were applied for generating the electroosmotic flow (EOF). For this reason, glasses, which have excellent EOF properties, started to be the preferred material for CE-related applications [21]. Additionally, glasses exhibit exceptional optical characteristics and well-understood surface chemistries, which impelled their widespread use for a multitude of microfluidic applications. However, the price associated with machining this substrate and the raw material cost is prohibitively high.

2.2 Polymer or Plastic Microfluidics

Due to the complex and diverse nature of the microfluidic applications, a variety of criteria is to be taken into consideration when choosing a substrate [12, 39]:

- simplicity of fabrication and machinability;
- purity and low-cost material availability;
- compatibility with chemical and biological reagents;
- suitable mechanical, chemical, and electrical properties;
- optical transparency;
- bondability and ability to encapsulate.

Presently, glassy materials are still preferred for electrokinetic flow applications due to their chemical inertness, their reliable polarity of charging, as

well as their transparency in visible and infrared (350 to 2500 nm). However, the cost constraints compelled researchers to find new materials other than silicon, glass, quartz, or metal that are more suitable for the whole host of microfluidic applications.

Polymers and plastics (i.e., polymers containing certain additives), although not a perfect match for all the above requirements, owing to their availability in pure forms at low cost, their broad range of material properties, and their simple machinability and moulding, started to be used as substrates for microfluidic chips from the mid-1990s [11, 12, 40]. Polymers are made of large molecules, composed of repeating structural units (monomers) interlinked by covalent chemical bonds. Typical polymers have a high molecular mass. They can occur naturally or can be formed via polymerization reactions. Based on their properties, polymers can be classified as thermoplastics (crystalline or non-crystalline), elastomers (rubbers), and thermosets (duraplastics). Thermoplastic polymers (e.g., polyethylene (PE) and polystyrene (PS)), as opposed to thermosets (e.g., Bakelite), can be melted on application of heat because they are not highly cross-linked. Elastomers (e.g. poly(dimethylsiloxane) (PDMS)) are very weakly cross-linked, and show a high degree of elasticity.

The first attempts at fabricating microchannels in plastic, which used a computer-controlled milling machine, were only capable of fairly large features (approximately 800 μm). Unfortunately, fluidic channels with large dimensions lead to an undesired turbulent flow [41]. Advances in technology permitted the

fabrication of much smaller diameter channels. Techniques such as hot embossing or imprinting [42-46], injection moulding [44, 47], soft lithography [48, 49], laser photoablation [50, 51] , x-ray lithography [52], ion beam etching with Ar^+ ions [53], and plasma etching [54] allowed the creation of much finer microfluidic channels, some of them with features as small as 1.5 μm. Further, all these techniques permit a wide range of geometries to be implemented.

A compilation of differences between silicon, glass, and plastics is reported in table 2-1.

Table 2-1: Materials of construction for electrokinetic microfluidic devices reproduced from [37].

	Silicon	Glass/Fussed Silica	Plastics
Thermal conductivity (cal/cm×s×°C)	0.35	~2×10^{-3}	4.5×10^{-4}
Bioassay compatibility	fair (oxide/nitride surface layer)	fair	very good
Optical detection	visible/UV: strong absorbance IR: transparent	glass: very good fused silica: excellent	poor to very good (varies according to polymer choice and wavelength)
Microfabrication	many well-developed approaches	isotropic wet etching only	silicon or glass mastering plus replication techniques; direct methods (ablation, dry etching)
Feature aspect ratio (depth: width of microchannel)	<0.1 - 40	<0.5	dependent on master for replication methods
Manufacturing methods	well developed	need development	well developed
Cost	inexpensive (small single devices) to expensive (large-area device arrays)	moderately expensive	inexpensive

Note, the key advantage plastics offer over silicon and glass is the cost. Although for chip sizes that are small (~1 cm^2) microfabrication of silicon or glass is not that expensive, for lager fluidic devices (~100 cm^2) the cost increases significantly. The latter devices are essential for applications, such as parallel screening a large number of pharmaceutical substances [11] or DNA sequencing [55]. Manufacturing these devices out of plastic is inexpensive enough to render them disposable after a single use. This approach is also a solution to applications where cross-contamination is of concern. Another key advantage of using plastics, not obvious from the above table, is that the manufacturing time is dramatically reduced in comparison to its silicon/glass/metal counterpart.

2.3 PMMA Microfluidics

A wealth of polymers and plastics, with a variety of physical and chemical properties, are fit for different kinds of microfluidic applications. The list of polymers that have been commonly used in microfabrication include poly(dimethylsiloxane) (PDMS) [56, 57], polycarbonate (PC) [58], poly(ethylene terephtalate) (PETE) [51, 59], polyimide (PI) [60], polystyrene (PS) [51], polypyrrole (PPy) - a conductive polymer - [61], poly(methyl methacrylate) (PMMA) [16, 62, 63], etc. Table 2-2 below highlights their characteristic properties.

Table 2-2: Properties of different polymers. The data was compiled from [64].

	PDMS	PC	PETE	PI	PMMA
Density ρ (kg/m^3)	1300	1200	1370 - 1380	1430	1170 - 1200
Tensile strength (MN/m^2)	-	52 - 62	66	68	45 - 72
10^5 x Coeff. linear expansion (°C)	8 - 30	6.6	6	4 - 5	5 - 9
Heat Capacity (J/g×K)	-	1.17 - 1.25	1.25	1.12	1.5
Thermal Conductivity (W/m×K)	0.15 - 0.32	0.19	0.29	-	0.17 - 0.25
Refractive index	1.43	1.59	1.54	translucent	1.48 - 1.50
Resistivity (Ω×cm)	10^{14} - 10^{15}	10^{16}	10^{16}	>10^{16}	>10^{14}
Dielectric constant	2.7	2.97 - 3.17	3.25	3.4	3.3 - 4.5

Arguably, the most used polymeric material by the microfluidics community, at least from 1990s on, is PDMS. Although its micromoulding was reported in the 1970s [65] and its use for biological-cell-related applications in the 1980s [66], its widespread use was promoted essentially by the wealth of publications generated by Prof. George Withesides' group at Harvard University. Simple or complex (i.e., multilayered) microfluidic systems could be easily fabricated in PDMS, while its transparency from 240 to 1100 nm allows optical detection to be performed. Quake's (Stanford University) and Mathies' (University of California Berkeley) groups created micromechanical valves out of it, taking advantage of its elastic properties. However, PDMS has some significant drawbacks: it absorbs either hydrophobic molecules from the solution [67] or hydrocarbons from the solvents [68]. Additionally, water easily permeates PDMS

[69] and replication of features smaller than 500 nm proves to be problematic [70].

In spite of the attractiveness of PDMS for microfluidics, our choice of material was PMMA. This decision was primarily based on reports of PMMA being the least hydrophobic of the most common plastic materials available [71]. Additionally, PMMA offers high transparency and very low autofluorescence over a wide spectral range [72], making it an ideal material for configuring microfluidic systems with integrated optical detection.

Chemically, PMMA is a very stable[2] [73, 74], linear[3] thermoplastic, resistant to most acids. In commercial applications, PMMA is a viable alternative to glass due to its high optical clarity and UV blocking capabilities [75]. Further, PMMA displays a high degree of impact resistance and, as opposed to glass, it does not shatter; instead, it breaks into large dull pieces on impact. PMMA's glass-transition temperature[4] is relatively low, approximately 105 °C [76-78], and causing a low heat-deflection temperature. Note that many of the chemical and mechanical properties of pure PMMA vary with the molecular weight distribution. In addition, for commercial PMMA, these properties can be modified through the addition of anti-yellowing agents or other additives.

[2] A stable polymer is, by definition, a polymer that remains polymerized at low subunit concentrations.

[3] A linear polymer is, by definition, a polymer in which the monomers are linked in a single chain that does not have any branches nor cross-linked structures.

[4] The glass transition temperature is, by definition, the temperature at which an amorphous solid (e.g., glass or polymer) becomes reversibly brittle on cooling, or soft on heating. The glass transition temperature depends on the molecular weight distribution.

The most used method for fabricating microchannels with high accuracy using thermoplastics and elastomers is micromoulding, which is accomplished either by replica moulding (soft lithography) [57, 80, 81], hot embossing [82, 83], or injection moulding [44, 82, 84]. Most of these methods, however, require the use of a master, which introduces extra fabrication steps and, most of the time, expensive infrastructure. Additionally, undercuts [5] in thermoplastics, which are sometimes very useful for microfluidic devices, cannot be fabricated using the traditional technologies. Further, the mould has a limited life, and the interface chemistry between the tool surface and the substrate polymer sometimes introduces a chemical or physical bond [42], which is detrimental to the final, desired, shape of the substrate. Should release agents be introduced to assist the mould release, microchannel contamination or an increase in substrate autofluorescence can occur.

To simplify the fabrication of microchannels, we have devised a simple approach that uses inexpensive resources. The proposed method is based on lithographical patterning of PMMA.

2.4 PMMA Patterning Through Exposure and Development

Creating a pattern in PMMA involves a two-step process. First, the substrate is irradiated selectively through a hard metal mask. Second, the irradiated PMMA is removed by dissolution, leaving behind the desired structure.

[5] Undercuts are structures in the polymer with overhanging edges.

2.4.1 Exposure of PMMA

PMMA has the merit of being the first positive resist to be used in advanced radiation microlithography [17]. The main mechanism through which the PMMA is patterned with a latent image is cleavage of chemical bonds. Bond cleavage, in both the main chain and in side groups, is the result of the absorption of high-energy radiation. Main chain scissions lead to a decrease in the average molecular weight, which, in turn, leads to an increase in PMMA solubility. Cleavages in side-groups create assorted volatile (such as H_2, CO, CO_2 and CH_4) and non-volatile products, leading to changes in other physical properties, such as the modification of the refractive index [85]. Mathematically, the number average molecular weight (a.k.a. fragmented molecular weight) of the exposed substrate can be calculated using [13, 86-89]:

$$M_f = \frac{M_n}{1 + \frac{g \cdot \varepsilon \cdot M_n}{\rho \cdot N_A}} \quad , \qquad \text{Equation 2-1}$$

where, M_n is the number average molecular weight, ρ is the density of the substrate, N_A is Avogadro's number, ε is the absorbed energy density, and g is the efficiency with which absorbed energy is converted to main-chain scissions. The ratio $\frac{g \cdot \varepsilon}{\rho \cdot N_A}$ represents the density of the main chain scissions. A graphical representation of equation 2-1 is shown in figure 2.1.

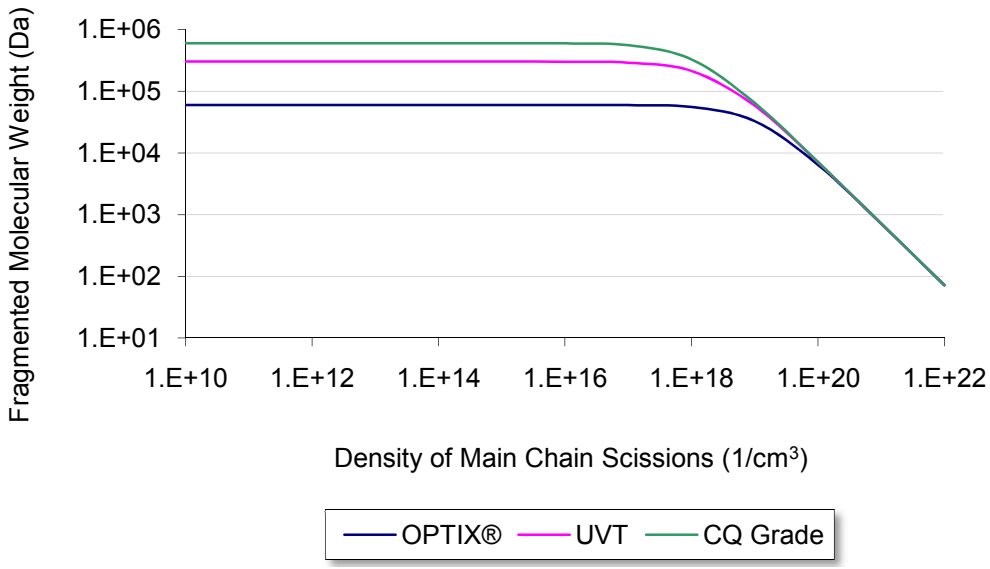

Figure 2-1: Fragmented molecular weight vs. density of main chain scissions. Initial number average molecular weights of 60 (OPTIX®), 300 (UVT), and 600 (CQ Grade) kDa were chosen for representation (adapted from [90]).

From small to large, the initial (i.e., before exposure) number average molecular weight of the three plots above corresponds to OPTIX®, UVT OP-4, and CQ grade PMMA samples. As discussed in section 3.2., those were the substrates of choice in which microchannels were created.

Radiation sources used with PMMA include: gamma rays [91, 92], X-rays [93, 94], electron beam [95, 96], proton beam [97], ion beam [98, 99], and deep-UV [14, 85, 100-102].

Due to changes in sensitivity, PMMA is used as a resist mostly with radiation sources more energetic than deep-UV. Even with those energetic sources, PMMA requires long exposure times [23, 103, 104]. However, PMMA can be exposed using ultraviolet radiation with a wavelength of 254 nm, even

though deep-UV is considerably less efficient than other radiation sources at producing main-chain scissions.

Most of the work presented in the literature on PMMA irradiation in the deep-UV involved photoablation using either ArF (193 nm) or KrF (248 nm) excimer lasers [105-109]. In the literature, the sensitivity of PMMA to deep-UV irradiation is considered to be at its maximum at 220 nm [110]. For wavelengths longer than 240 nm, the absorptivity of PMMA is very low [13], which is the reason why these wavelengths did not stir much research interest. Nevertheless, the work herein demonstrates that the PMMA sensitivity at 254 nm is not negligible. The reason behind using this particular wavelength is that producing 254 nm radiation using low-pressure mercury vapour lamps is inexpensive.

The low sensitivity to visible and near-UV spectra is not necessarily a disadvantage; it can be useful for exposing thicker substrates more uniformly. The Beer-Lambert law, which relates the absorption of light to the properties of the material, states that

$$T = \frac{I}{I_0} = \exp(-\alpha z), \qquad \textbf{Equation 2-2}$$

where T is the transmission (or transmissivity), I_0 and I are the intensity (or power) of the incident light and the light travelling a distance z inside the material, respectively, and α is the absorption coefficient of the substance. A uniform dose inside the material implies $\frac{I}{I_0} \to 1$; this uniformity happens when the

absorptivity α of the material approaches zero. The uniform exposure of the substrates is very important for high aspect ratio lithographic processes [101, 111], such as LIGA[6] [112-115].

2.4.2 Development of PMMA

The irradiated PMMA is removed, usually by dissolution, in a developer bath. Dissolution is facilitated by previously induced polymer backbone scissions, lower molecular weight polymer being more readily dissolved by the developer than the unexposed PMMA. This property is, in fact, how the developer is chosen: it must be a poor solvent for unexposed PMMA, but able to dissolve low molecular weight PMMA [116]. Additionally, the developer must be kinetically a good solvent – so that it minimizes the undercut through a rapid development [117] – while, at the same time, thermodynamically a poor solvent – so that it minimizes swelling of the PMMA. Consequently, typical PMMA developers are binary mixtures of good and bad PMMA solvents. Their ratio dictates the thermodynamics and the kinematics of the dissolution process.

Probably the most important parameter for characterizing the development is the dissolution rate ratio, *DRR*. It is defined as the ratio between the dissolution rates of the exposed, $R_{EXPOSED}$, and the unexposed, $R_{UNEXPOSED}$, PMMA:

[6] LIGA is a German acronym for **Li**thographie, **G**alvanoformung, **A**bformung, meaning lithography electroplating and moulding.

$$DRR = \frac{R_{EXPOSED}}{R_{UNEXPOSED}}. \qquad \textbf{Equation 2-3}$$

The dissolution rate, which is directly determined for a given solvent by the fragmented molecular weight, can be approximated by the empirical formula [86-89, 118]

$$R = R_0 + \frac{\beta}{M_f^{\alpha}}, \qquad \textbf{Equation 2-4}$$

where M_f is the fragmented molecular weight, while R_0, α, and β are empirical constants. Replacing for $R_{EXPOSED}$ and $R_{UNEXPOSED}$ in equation 2-3, the dissolution rate ratio becomes

$$DRR = \frac{R_0 + \frac{\beta}{M_f^{\alpha}}}{R_0 + \frac{\beta}{M_n^{\alpha}}}. \qquad \textbf{Equation 2-5}$$

Considering R_0 negligible in the above equation yields

$$DRR \approx \left(\frac{M_n}{M_f}\right)^{\alpha}, \qquad \textbf{Equation 2-6}$$

where M_f and M_n are the number average molecular weights of the exposed and unexposed PMMA, respectively, while α is the developer kinetic solubility.

Historically, one of the most used developers for PMMA was a mixture of methyl isobutyl ketone (MIBK) and isopropanol alcohol (IPA) [101, 119, 120] at

room temperature. Various MIBK/IPA mixture ratios were reported, ranging from 1:4 [87], 1:3 [86-88, 119, 121-123], 4:6 [124], 1:1 [123, 125], to 8:2 [120]. Various ratios dictate the tradeoffs between contrast and sensitivity [123]. Increasing the concentration of MIBK in the developer solution increases the sensitivity, but sacrifices the contrast. Similarly, developer solutions were made from methyl ethyl ketone (MEK) and IPA [117, 118, 120, 126-128] or MIBK and methanol or ethanol [88, 117, 118, 127]. As well, MIBK alone was used as developer [101, 111]. For all the above, IPA can be used to quench the development process [119, 121, 129].

Another heavily used solvent, especially in LIGA [113-115], is the GG developer. The GG developer is an empirically found mixture made, by volume, of 15% water, 60% 2-(2-butoxyethoxy)ethanol, 20% tetrahydro-1,4oxazine (morpholine), and 5% aminoethanol [130-132]. Quenching for this developer uses DI water.

A relatively new developer is a mixture of isopropanol alcohol (IPA) and water [130, 133, 134]. Intriguingly, neither IPA nor water is a PMMA solvent on its own. The ratio that optimizes both, sensitivity and contrast, is 7:3 IPA/H_2O [135]. Although not as aggressive as MIBK/IPA, this developer has a more linear response [136]. Further, GG developer is very toxic [130] and MIBK/IPA developers introduce worm-like defects along the sidewalls [137] and cause the PMMA to swell [130]. Therefore, we determined to use 7:3 IPA/H_2O as developer for our work.

Worth noting is that ultrasonics can help increase the dissolution rate of PMMA [138, 139] because they promote mixing and they reduce the viscosity of the polymer-solvent solution through shear thinning [138]. Ultrasonics, however, can damage small or delicate features if not carefully used.

3 PROCESS DEVELOPMENT

Although PMMA can be patterned using a variety of exposure sources, as discussed in the previous chapter, deep-UV at 254 nm is of a particular interest because it is relatively inexpensive. Additionally, deep-UV sources can be readily scaled to large area exposures of commercial grade PMMA.

This chapter focuses on the core of the process, presenting its constitutive elements.

3.1 Irradiation Source

The PMMA exposure in this thesis was performed using a novel wavelength, namely 254 nm. Though recent papers reported the exposure of thin layers of spin-coated PMMA using 254 nm [14, 15], this wavelength has not been well reported in the literature. In fact, until the publication of our work [16], no reports were published on patterning commercial acrylic using this particular wavelength.

The 254 nm radiation source for this thesis work was obtained using the Stratalinker 2400 UV crosslinker, which is manufactured by Stratagene [18]. The low pressure mercury vapour lamps used by the Stratalinker 2400 UV crosslinker provide non-collimated radiation with a nominal power of 4 mW/cm^2 and a

spectrum whose strongest peak is at 254 nm. Each unit is equipped with five 15 W bulbs and allows two modes of operation: energy mode in which the desired dose in μJ/cm^2 is set, and time mode in which the desired exposure time in minutes is entered. The maximum exposure dose in energy mode is too low to affect the PMMA significantly, so all exposures used the time mode. The external dimensions of the Stratalinker 2400 are 58×40×25 cm, while the total area inside the box that can be irradiated is 1,560 cm^2. The Stratalinker 2400 can expose over twenty 3"×3" (7.6×7.6 cm) samples simultaneously.

3.2 Substrates

Our fabrication experiments used inexpensive commercial PMMA for the substrates. Plaskolite's OPTIX® was chosen, not only for its good mechanical and optical proprieties [140] (see appendix B) that would allow a wide variety of microfluidic applications, but also for its low price (approximately \$0.005 cm^{-2}). OPTIX® is an atactic[7] PMMA of a relatively low molecular weight compared with other forms of PMMA available on the market. Gel permeation chromatography (GPC), using tetrahydrofuran (THF) as the solvent, was performed to determine the molecular weight distribution[8]. The weight average molecular weight measured against a polystyrene standard was found to be M_w = 55.7 kDa, with a

[7] In an atactic macromolecule, the substituents are placed randomly along the chain, whereas in a tactic macromolecule, all the repeating units are identical.

[8] Polymers do not have a single molecular weight because their chains vary in length.

polydispersity[9] of 1.48. The weight average molecular weight gives a measure of the molecular weight of a polymer. By definition, it is calculated by

$$M_w = \frac{\sum_i N_i M_i^{\,2}}{\sum_i N_i M_i}, \qquad \textbf{Equation 3-1}$$

where N_i is the number of molecules of molecular weight M_i.

In general, for micro-fabrication, PMMA of a much higher molecular weight is typically used [99, 141, 142], particularly when used as a resist. To compare the performance of OPTIX® with a PMMA formulation closer to those used in microfabrication, a clinical quality (CQ) grade PMMA that was free of additives was purchased from GoodFellow [143] (see appendix B). Through GPC analysis, its weight average molecular weight was found to be 628 kDa, with a polydispersity of 1.1. Another type of commercial PMMA that we considered for comparison purposes was an ultraviolet transmitting tanning (UVT) bed acrylic Acrylite® OP-4 [144], which was acquired from CYRO Industries (see appendix C for properties). Its weight average molecular weight was determined to be M_w = 305,807, with a polydispersity index of 1.03.

3.2.1 Optical Absorbance

As mentioned in chapter 2 (see equation 2-2), having a low absorptivity substrate is desirable because this facilitates a uniform exposure of the volume.

[9] The polydispersity index is the ratio of the weight average molecular weight to the number average molecular weight. The number average molecular weight is determined by measuring the molecular weight of n polymer molecules and dividing the result by n.

As such, absorbance measurements would provide valuable information about the sensitivity of various PMMA substrates to illumination with 254 nm.

Thin films of three different molecular weight PMMA were cast and exposed to gradually increasing doses of deep-UV, and the absorbance was measured using a Varian UV-Visible spectrophotometer (Cary 300 Bio). One PMMA casting solution of 495 kDa molecular weight, 11% in Anisole, was purchased from MicroChem. This PMMA is free from additives and, although it has not been used for the rest of our work, it was chosen for comparison purposes. The other two types of PMMA were OPTIX® and UVT OP-4, both 6% in Anisole.

PMMA was cast on top of 3"×3" (7.6×7.6 cm) glass slides. The casting solutions were then hardened through a two-step thermal process using a Torrey Pines Scientific model HP30 hotplate. The first step was a 3-hour bake at 130 °C, while the second step was a 1-hour bake at 150 °C, after which the films were cooled gradually, naturally to room temperature. In order to maintain a rich solvent vapour atmosphere, which would facilitate a gradual, as opposed to sudden, evaporation of the anisole from the bulk, a funnel was used to cover the glass slide. This technique alleviates the stress in the film, rendering clean, crack-free, homogenous films because the anisole leaves the substrate gradually, condensing on the internal side of the funnel. The role of the second thermal step is to ensure the complete removal of the solvent from the film.

Due to their different coefficients of thermal expansion with respect to the glass and a very poor adhesion to it, the acrylic films could be easily peeled off the glass slides. The films were then irradiated with deep UV doses in 72 J/cm^2 increments, up to 720 J/cm^2. Measurements were taken at the same location on the film immediately after the exposure.

To determine the absorption coefficient, equation 2-2 can be re-written as

$$\ln\left(\frac{I}{I_0}\right) = \alpha \cdot z \,. \qquad \textbf{Equation 3-2}$$

Since the thickness of the substrate *z* can be measured from the sample, the absorption coefficient of the substance can be determined. Figure 3.1 below reports the results.

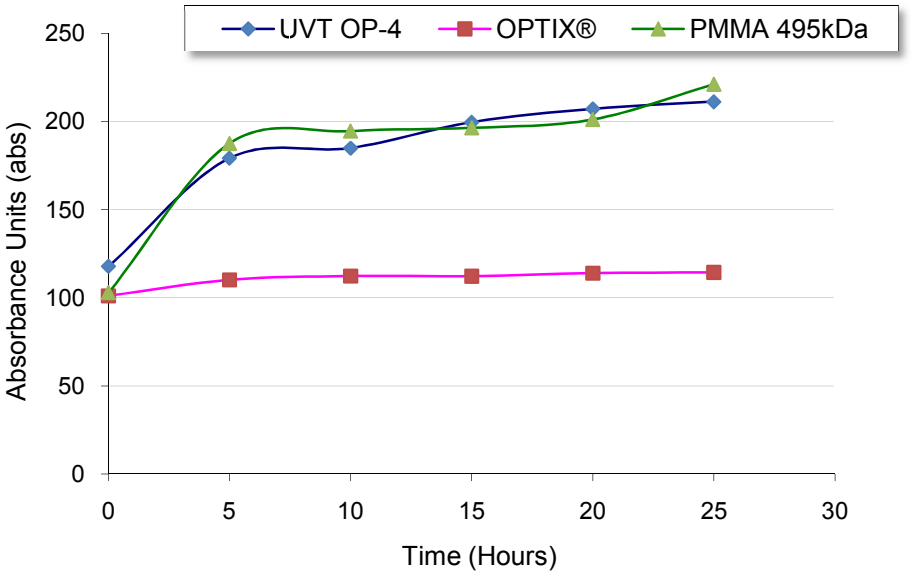

Figure 3-1: Absorbance of three different types of acrylic versus exposure time. Each 5 hours of exposure correspond to a dose of 72 J/cm^2.

As a general trend, the results are in agreement with the literature reports [145] of increased absorbance after illumination with UV light. This increase is more pronounced for UVT and PMMA 495 kDa but much less so for OPTIX®. It is worth mentioning, however, that the increased absorption is mainly due to the ongoing photooxidation reactions during the exposure [146]. For some commercial acrylics, additives are added to the bulk to enhance this process. After more than 30 hours of exposure do deep-UV, the cast films started to warp significantly and fine scratches developed randomly across the surface. Additionally, small portions of the films frequently shattered when the films were taped down for having the absorption measurements taken. All the above phenomena led to an unreliable absorption reading and, consequently, we decided not to report readings taken after twenty five hours of deep-UV exposure.

Based on the absorbance measurement, clearly, OPTIX® is a very good candidate for patterning high aspect ratio features because it has the lowest absorbance readings. Nevertheless, as discussed in chapter 2 (see equation 2-6), the dissolution rate ratio depends on the molecular weight values of the exposed and unexposed areas. Consequently, having a high molecular weight PMMA is desirable so that the dissolution rate ratio can be maximized. This is not the case with OPTIX® for it has the lowest number average molecular weight of the three samples.

The data associated with the above graph is given in appendix D.

3.3 Process Steps

This section describes the succession of fabrication steps for patterning the PMMA and creating the microfluidic devices.

3.3.1 PMMA Patterning

The basic fabrication sequence for creating microfluidic channels is shown in figure 3.2. Each step is described in more detail in the body of this section.

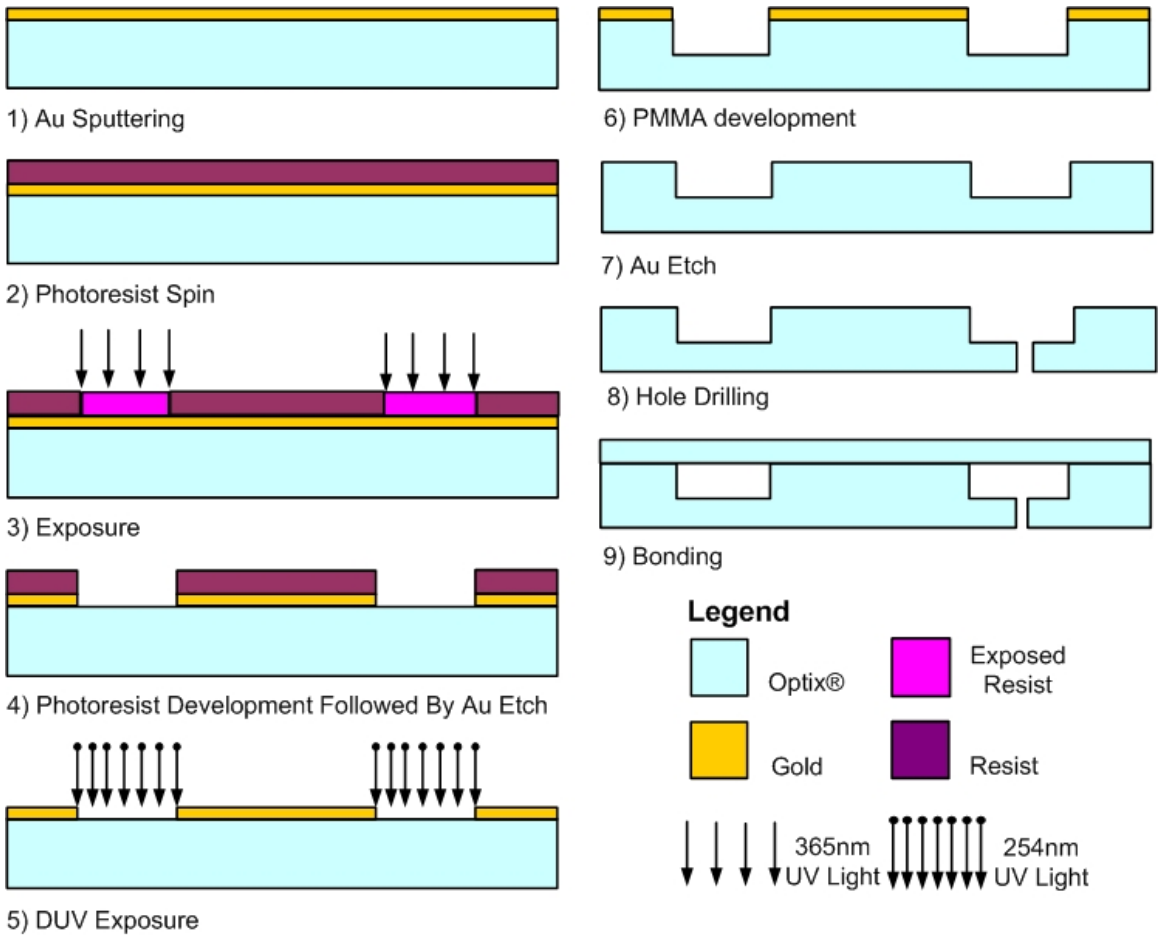

Figure 3-2: Deep-UV exposure of PMMA: process steps.

All PMMA substrates came in 1'×1' (30.8×30.8 cm) sheets from which 3"×3" (7.62×7.62 cm) samples were cut. The samples were cleaned with deionised water (DI) and a mild dishwasher gel; they were then immersed for 10 minutes in a methanol bath to remove any oily residues.

The samples were dried with N_2 gas and then sputtered with 100 nm of gold at 80 W using a Corona Vacuum System sputterer. The gold layer acts as a mask for subsequent deep UV patterning. Gold was selected for historical reasons; many other metals, such as chromium, aluminium or copper, could also be used for the hard mask. It is worth mentioning that, despite the common belief of poor adhesion of gold to polymers, no problems with delamination were observed. After metal deposition, Shipley 1813 photoresist was spun-on at 4000 rpm for 30 seconds. Because the PMMA could warp if baked above 100 °C, the photoresist baking temperature was kept below 75 °C. The sample was exposed through a contact mask using an i-line[10] source and developed in MF-319 developer. A gold etch was completed using TFA gold etchant from Transene Company, Inc. Following the gold etch, the photoresist was removed by using a 60 second blanket exposure followed by another development in MF-319. The removal of the photoresist prevents damage to the OPTIX® by organic solvents. At this point, the samples were ready to be exposed to deep UV. Figure 3-3 shows a PMMA sample after gold patterning.

[10] A high intensity line at 365 nm in the spectrum of a UV lamp is referred to as "i-line."

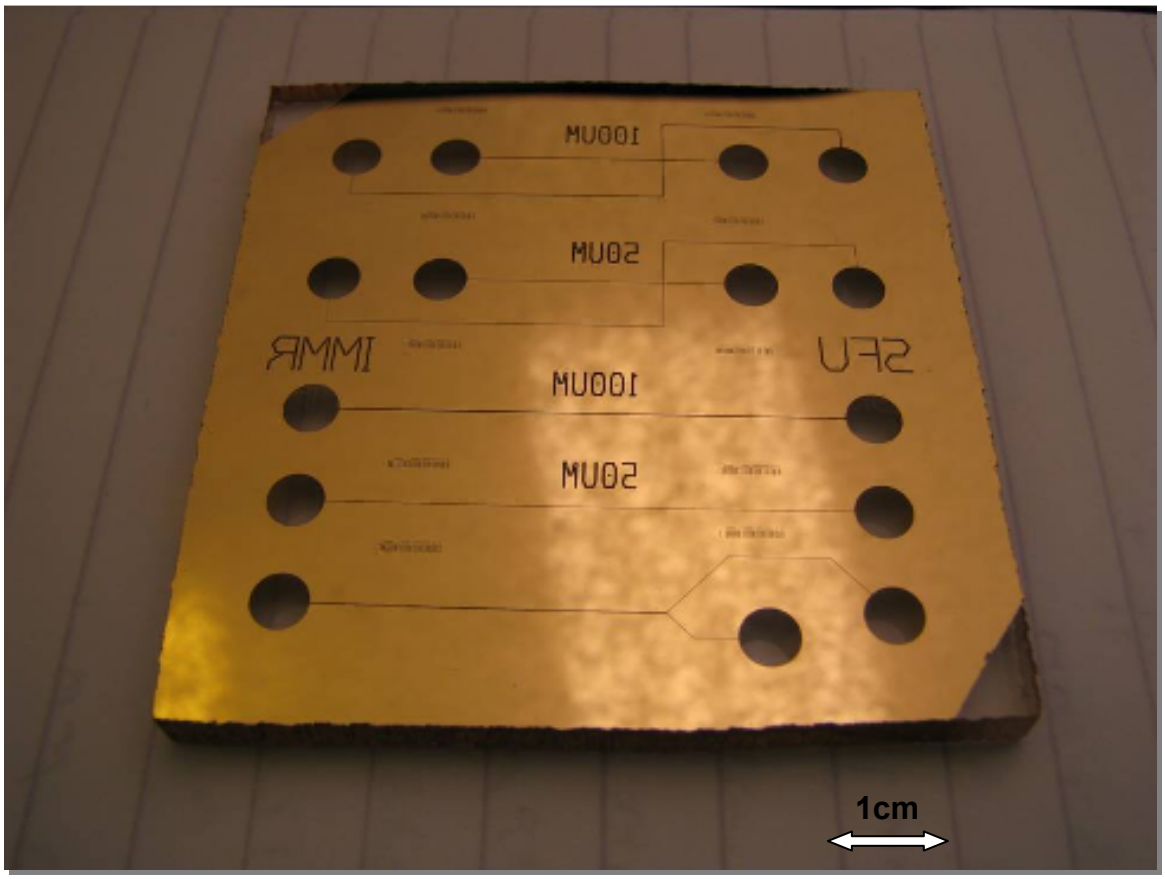

Figure 3-3: Photograph of a PMMA sample on which the gold hard mask was sputtered and patterned.

The PMMA samples were exposed using the Stratalinker 2400 UV crosslinker. Although the exposure power is low, this disadvantage is partially offset by the large number of substrates that can be exposed simultaneously. Figure 3-4 shows the Stratalinker, with PMMA substrates inside, ready for exposure.

Figure 3-4: Photograph of Stratalinker 2400 used as a deep-UV radiation source.

The PMMA substrates were divided into four groups, whose exposure times varied from 15 h to 60 h in 15 h increments. Each 15 h increment corresponds to a nominal dose of 216 J/cm^2. After exposure, samples were transferred to a developer bath, which was a mixture of 7:3 IPA:H_2O at 28 °C. Throughout the development, the bath temperature was monitored by a steel enclosed thermocouple and maintained to an accuracy of ±2 °C by a Torrey Pines Scientific hotplate. Figure 3.5 shows the development bath on top of the hotplate.

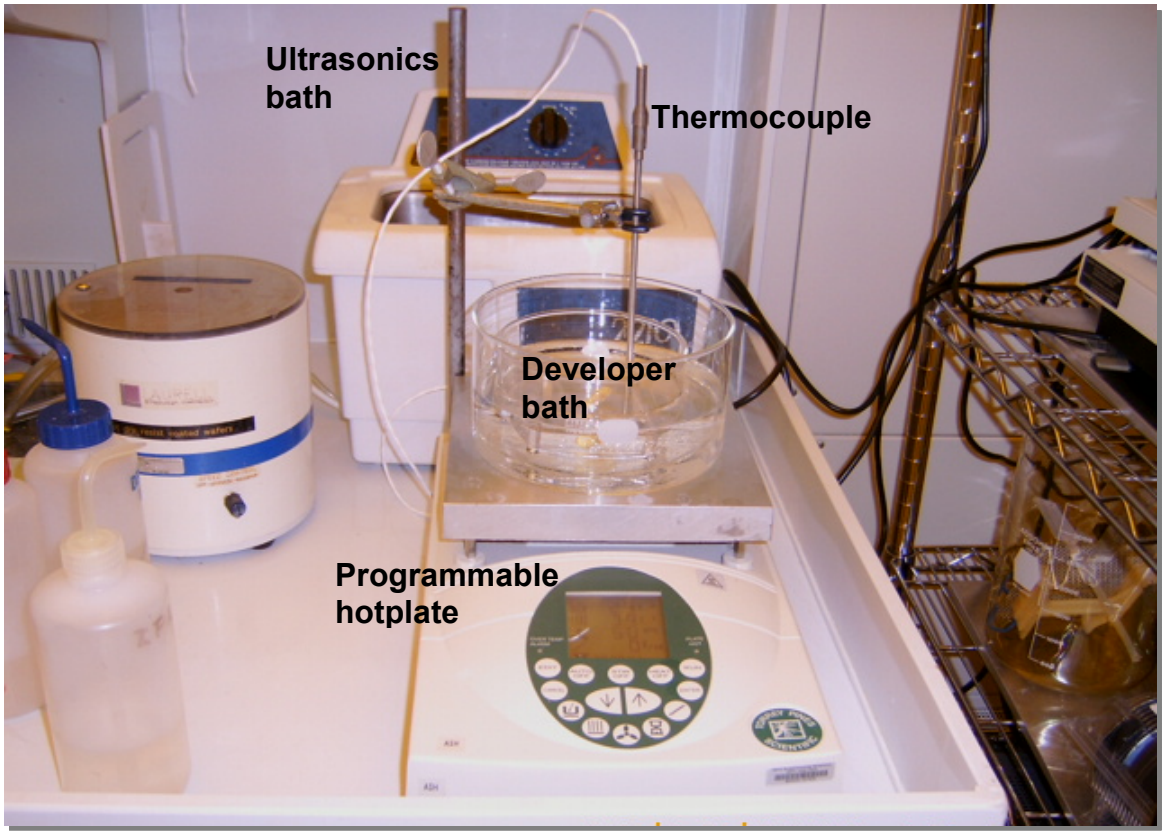

Figure 3-5: Development setup consisting of a bath - whose temperature is monitored by a thermocouple – on top of a programmable hotplate.

Occasionally, the samples were given a slight manual agitation. The development time for each group of samples was 1 h, but the development was split into 10 min segments. At the end of each segment, the development was quenched in an ultrasonic IPA bath at room temperature (18 °C) for 10 s, after which the samples were sprayed with IPA for another 10 s, and then blown dry with N_2. The depth of both the channels and reservoirs (inlets/outlets) was measured with an Alpha-step 500 profilometer. Measurements of the developed depth were taken for different exposure doses and development times. The recipe of the process is given in appendix E.

3.3.2 Microfluidic Device Fabrication

After each group of samples was developed for a total time of 1 h, the gold mask was stripped in TFA Gold Etchant. Then, 0.5 mm diameter ports were drilled into the PMMA, and world-to-chip interconnects in the form of polytetraflourethylene (PTFE) tubing were attached to them. The chemical inertness of the tubing was the main selection criteria.

The microfluidic channels produced in PMMA were sealed and then tested for leaks. Thermal bonding, loosely based on the previous work described in the literature [147, 148], was used to seal the patterned PMMA substrates to non-patterned ones. We experimented with two nearly identical procedures. In one procedure, bonding was completed at atmospheric pressure; in the other procedure, bonding was done at 15 kPa. The core of the procedures consisted in maintaining both the cover plate and the patterned substrate at 90 °C for 90min while pressed together (approximately 41 kPa) using a custom built vice, made out of two thick aluminium plates. The ovens used for the thermal bonding were Sybron Thermolyne type 1900 and Forma Scientific Vacuum Oven, model 3237, respectively.

The fluidic ports in the PMMA were connected using 0.45 mm inner diameter PTFE tubes to syringes (Hamilton 1002 TLL, 2.5 mL), which were hooked up to a Harvard syringe pump, model 11. The polyurethane tubes

were fixed to the PMMA using Loctite 495 glue. The syringe pumps contained dyed water to ensure fluid visibility in the channel. Running the dyed water at various flow rates through the microfluidic devices served as a leakage test. The pressure of the flow was monitored by connecting an Omega PX26-005GV pressure transducer in series with the liquid flow.

4 PROCESS CHARACTERIZATION

Using the recipe presented in the previous chapter a microfluidic device pattern was transferred into three different types of commercial PMMA samples. The differential solubility [13, 23] obtained by the exposure creates grooves in the PMMA. In short, PMMA behaves like a positive resist. Our developer of choice was a mixture of 7:3 IPA and DI water. The capabilities of this developer to dissolve zones of exposed PMMA is characterised in the first part of this chapter. Then conditions that can enhance the development rate, such as temperature of the solvent or its agitation, are discussed followed by considerations about issues of development for different geometrical profiles. The chapter concludes with a presentation of the test set-up and test results for an enclosed microfluidic system.

4.1 Dissolution Rates

Four OPTIX® substrates, which were exposed with multiple doses of 216 J/cm^2 of deep-UV, were developed for a total of 60 minutes. The substrates were brought out of the bath to have the depth measured every 10 minutes. The depths were measured at four different locations, either inside the channels or inside the reservoirs. Figure 4.1 summarizes the measurements (see appendix F for the data).

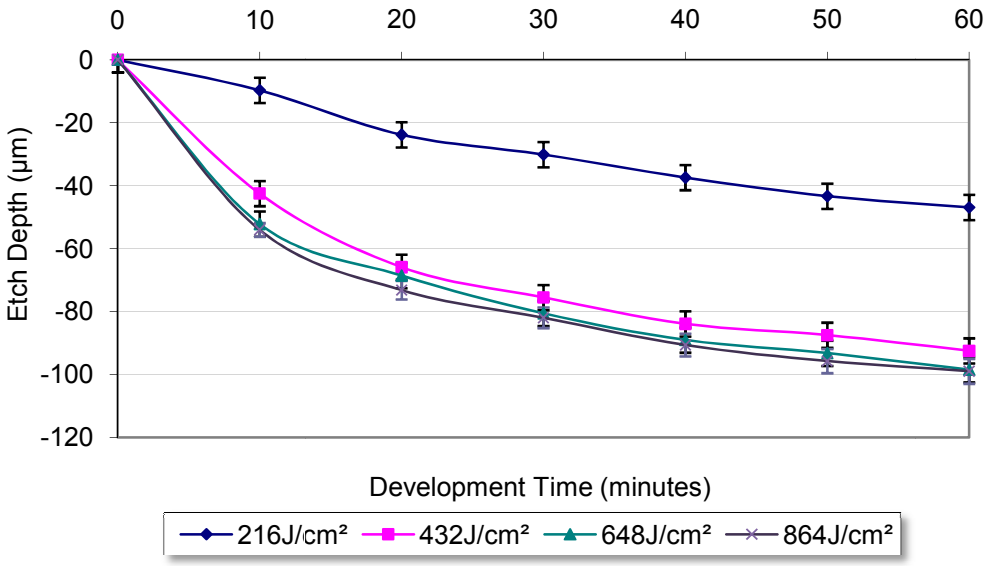

Figure 4-1: Etch depth versus time for OPTIX® PMMA exposed with multiple doses of 216 J/cm^2 of deep-UV.

The above procedure was repeated for OVT OP-4 acrylic. The results are shown in figure 4.2 (see appendix G for the complete data).

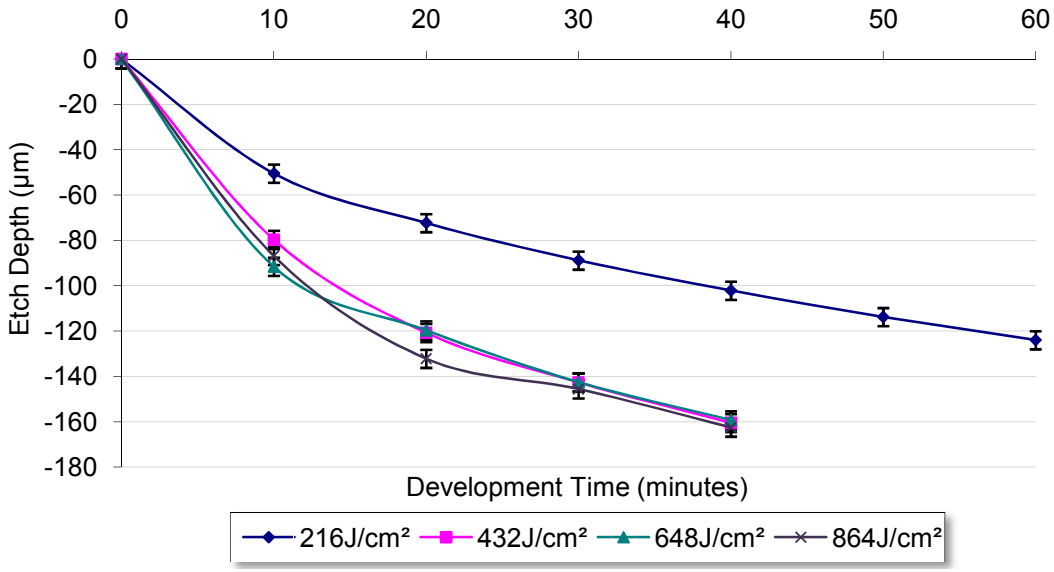

Figure 4-2: Etch depth versus time for UVT OP-4 PMMA exposed with multiple doses of 216 J/cm^2 of deep-UV

In the graph above, etch depths for more than 40 minutes of development are not reported because the maximum depth measurement capability of our profilometer is 150 μm.

Deep-UV irradiation facilitates dissolution in the developer bath because the molecular weight distribution of the PMMA is modified through main chain scissions. The number average molecular weight at a certain moment in time during the exposure depends on the absorbed energy density and on the efficiency with which this energy is converted into main chain scissions.

Because of the low coefficient of absorption of pure PMMA at 254 nm (5.6 cm^{-1}) [149], we originally expected that the dissolution rate would show very little dependence with depth. However, this hypothesis turned out not to be the case. This increased absorption is likely due to a combination of the additives used by the manufacturer and photo-oxidative products [145, 146].

The dissolution rate, as expected, increases with dose. However, exposure doses in excess of 432 J/cm^2 have a limited impact on the dissolution rate. The reason for this behaviour is currently unknown. One possible explanation is that the accumulation of chemical species from secondary chemical reactions, particularly the photo-oxidative products, increased the absorption of deep-UV by such a degree that exposure of the bulk PMMA was essentially quenched.

4.2 Effect of a Titanium Barrier Layer

To verify the hypothesis that oxidation of PMMA causes increased absorption of deep-UV radiation, as proposed at the end of the previous section, we added a thin layer of Titanium (Ti) as an oxygen barrier layer. These samples were exposed to deep-UV and the resulting etch depth was analyzed.

The purpose of the titanium layer is to prevent oxygen diffusion. However, we expect that some oxygen may still be present in the PMMA sample and it may also diffuse from the backside of the sample. A fair assumption is that the incorporated and the diffused oxygen quantity is quite small and, therefore, its contribution to photo-oxidative products can be neglected.

A 5-nm thick Ti layer was deposited on PMMA samples using a Corona Vacuum System sputterer running at 80 W power. The samples were then exposed to deep-UV and, after exposure, the titanium layer was removed by immersing the samples for 10 seconds in a solution of 1:10 $HF:H_2O$ at 50 °C.

Five groups of OPTIX® samples were given doses of 216, 432, 648, and 846 J/cm^2. The graph in figure 4.3 summarizes the measurements (full data is presented in appendix H).

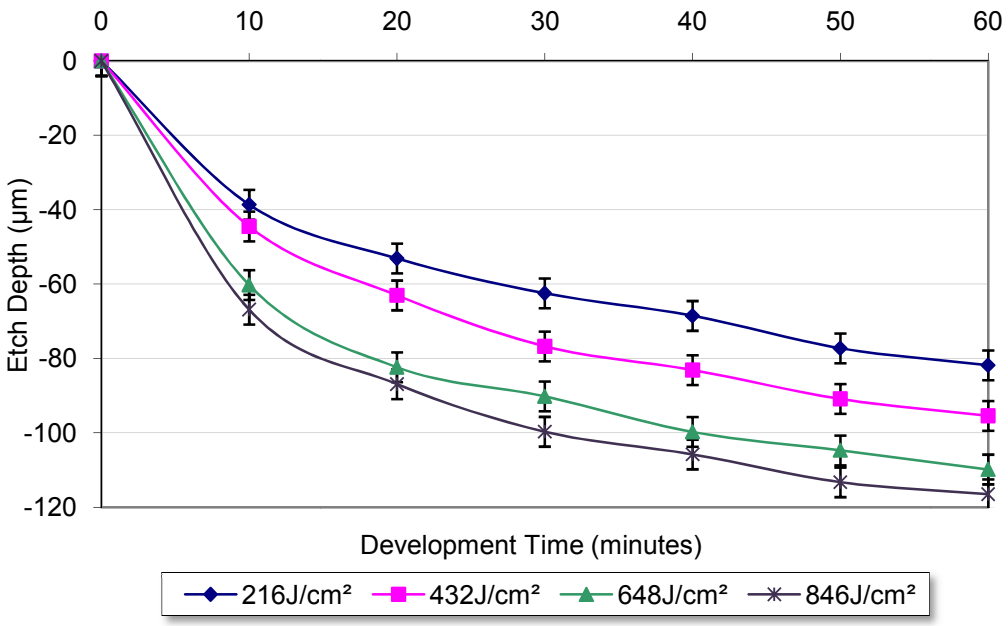

Figure 4-3: Etch depths versus time for OPTIX® PMMA exposed through a 5nm thick Ti barrier layer with multiple doses of 216 J/cm^2 of deep-UV.

Comparing the results in the graph above (full data in appendix H) with the ones in figure 4.1 (full data in appendix F) the increased etch depth when Ti is used is evident. As well, the graphs corresponding to exposure doses of 432 J/cm^2 or more of are more evenly spaced, a sign of deeper radiation penetration in the bulk. Therefore, clearly, the Ti layer helps to alleviate the exposure quenching noted in section 4.1. The accumulation of the photo-oxidative products still takes place, however, mainly due to the non-uniformity of the Ti film[11].

[11] This conclusion is the result of a discussion with Bill Woods, who performed the deposition. He mentioned that he could not reach a high enough vacuum level inside the sputtering chamber due to the substrate out-gassing. Consequently, the Ti layer likely had tiny holes in it.

4.3 Effect of Temperature and Agitation

The dissolution rate profile can be altered by modifying the developer temperature or by introducing agitation into the developer bath. Elevating the bath temperature considerably increases the dissolution rate, but our trials determined that the increased dissolution rate was at the expense of increased surface roughness of the channel bottoms. The working temperature was chosen to be 28 °C as this was the maximum temperature that retained a smooth surface independent of the exposure dose. Figure 4.4 shows the smooth profile of the channel after long development times.

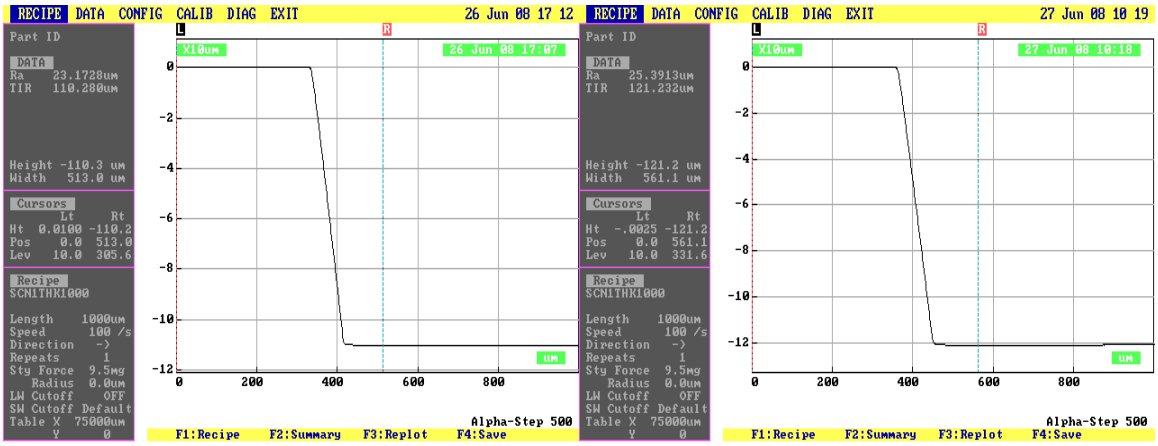

Figure 4-4: Profilometry measurements of developed PMMA after a 1080 J/cm^2 dose followed by 40 min (left) and 60 min (right) of development, respectively.

Additional dissolution rate trials were performed using a magnetic stirring rod in the developer bath. The speed was set to 400 rpm for a bath volume of 200 mL. Using a stirring rod increased the dissolution rate by approximately 20%. The stirring rod and the sample inside the bath must be properly centred otherwise the sample surface can become strongly uneven. Additionally, the

sample should be raised so that it is placed over the stirring rod. Figure 4-5 shows the developer bath setup, with the sample elevated on a stand-off and the stirring rod underneath the sample. There is no developer present inside the bath for a better clarity of the picture.

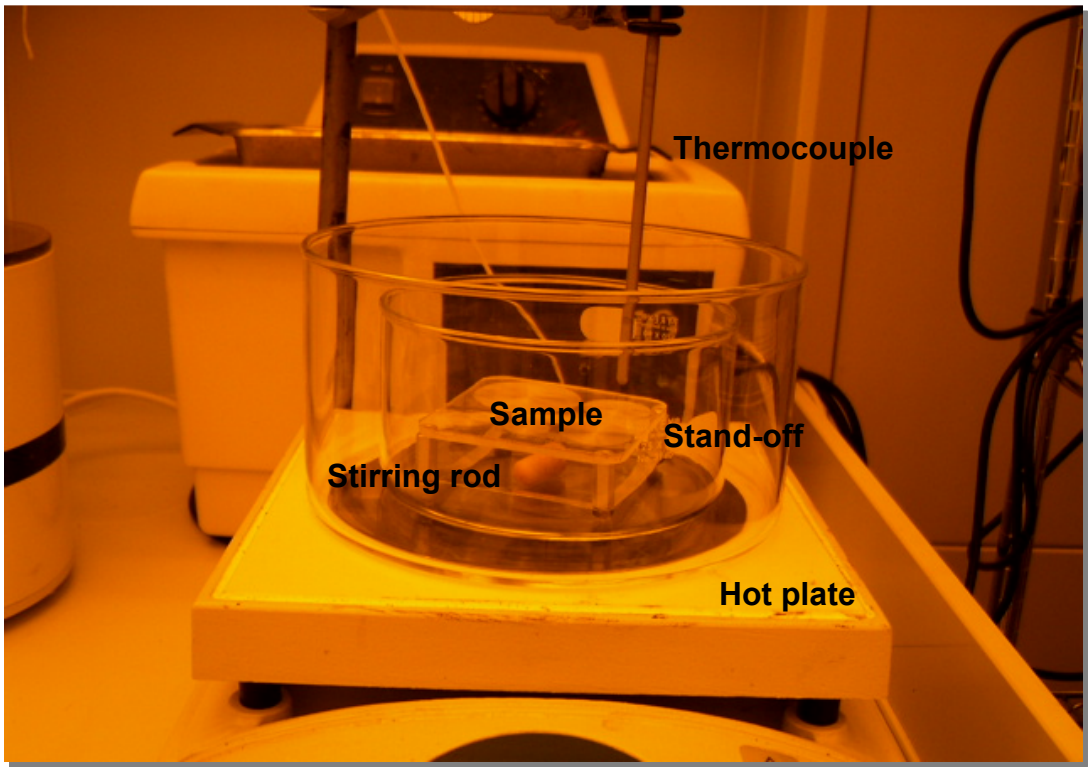

Figure 4-5: Developer bath setup when agitation is introduced during development.

Figure 4.5 shows the resulting etch depths versus development time while appendix I reports the associated full data.

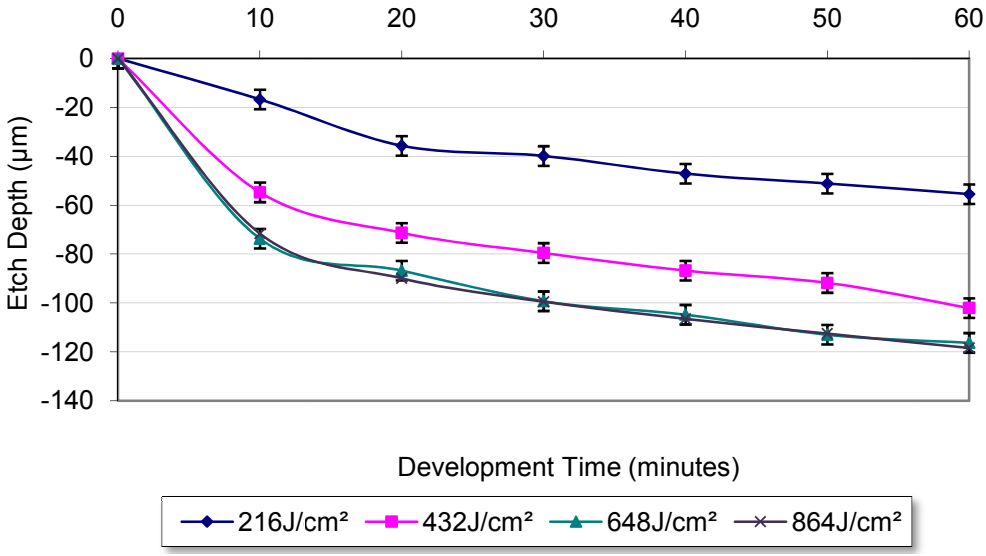

Figure 4-6: Etch depths versus time for OPTIX® PMMA exposed with multiple doses of 216 J/cm^2 of deep-UV. Development was performed with mechanical agitation.

UVT OP-4 PMMA was characterized in a similar manner. Figure 4.6 shows the results and appendix J contains the full data.

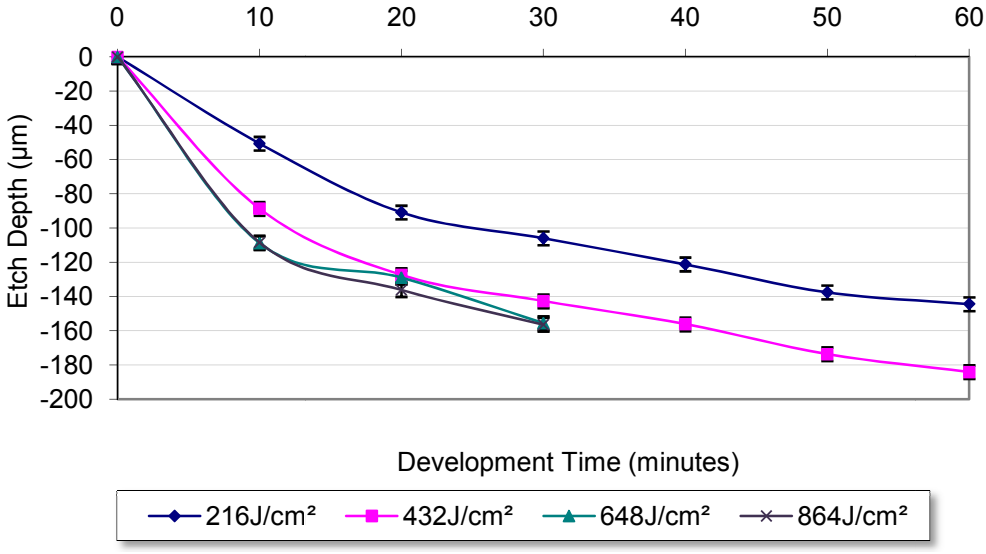

Figure 4-7: Etch depths versus time for UVT OP-4 PMMA exposed with multiple doses of 216 J/cm^2 of deep-UV. Development was performed with mechanical agitation.

4.4 Considerations on Aspect Ratio and Side Walls

Although the profilometry measurements demonstrate the uniformity of the geometry of the microfluidic channels, we are limited to channels having minimum dimensions of 50 μm. When smaller than 50 μm channels were patterned, different dissolution depths were observed. These depths could not be measured precisely because of the profilometer's stylus inability to reach the full depth on samples with extremely narrow gaps. Additionally, we noted that closely spaced features smaller than 10 μm were frequently missing after 20 min of development time. To test the development of very small features, a high molecular weight PMMA sheet was patterned and developed in a similar manner as the OPTIX®. Intuitively, higher molecular weight PMMA should show higher selectivity during development due to the much lower dissolution rates of the unexposed areas.

The high molecular weight PMMA was clinical grade (CQ) from Plaskolite, with a number average molecular weight of 628 kDa and a polydispersity of 1.1. A mask with minimum features of 2 μm, used elsewhere [150], was utilized for this test. For these samples, the deep-UV exposure dose was limited to 216 J/cm^2. After development, 10 nm of gold was sputtered on the sample in preparation for viewing the samples under a scanning electron microscope. Several scanning electron microscope (SEM) images of this sample are shown in figure 4.7.

The resulting images show that for the high molecular weight PMMA, a significant negative sidewall occurred at longer development times. This sidewall was not as obvious in the OPTIX® PMMA either because of poorer selectivity or because the aspect ratio of the channels was lower (a similar situation to that shown in figures 4.7 a) and 4.7 b)). Trenches wider than 20 μm had uniform depths, whereas narrower trenches were less deep. This reduction in depth

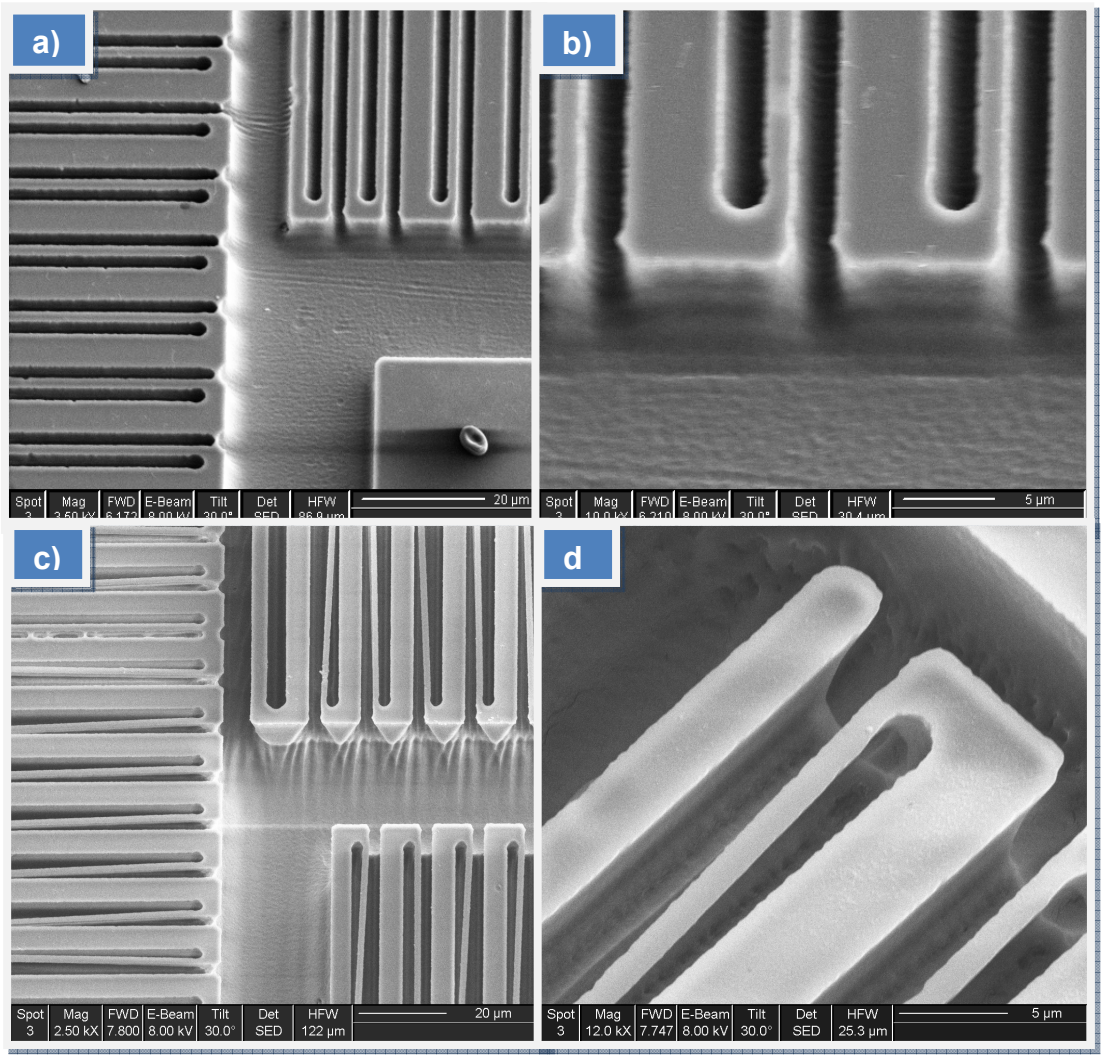

Figure 4-8: SEM images of patterned CQ PMMA after 10 min of development a) and b) and 50 min of development c) and d). Small features are completely undercut due to negative side walls.

is likely due to a combination of a lower received dose and mass transport limitations.

The negative sidewall is attributed to the non-collimated nature of the deep-UV light, and will limit the aspect ratio of the features produced when using an un-collimated light source.

4.5 Test of Microfluidic Channels

After bonding to create sealed channels, PTFE tubes were connected at one end to the reservoirs and at the other end to syringe pumps. A photograph of the test system is shown in figure 4.9.

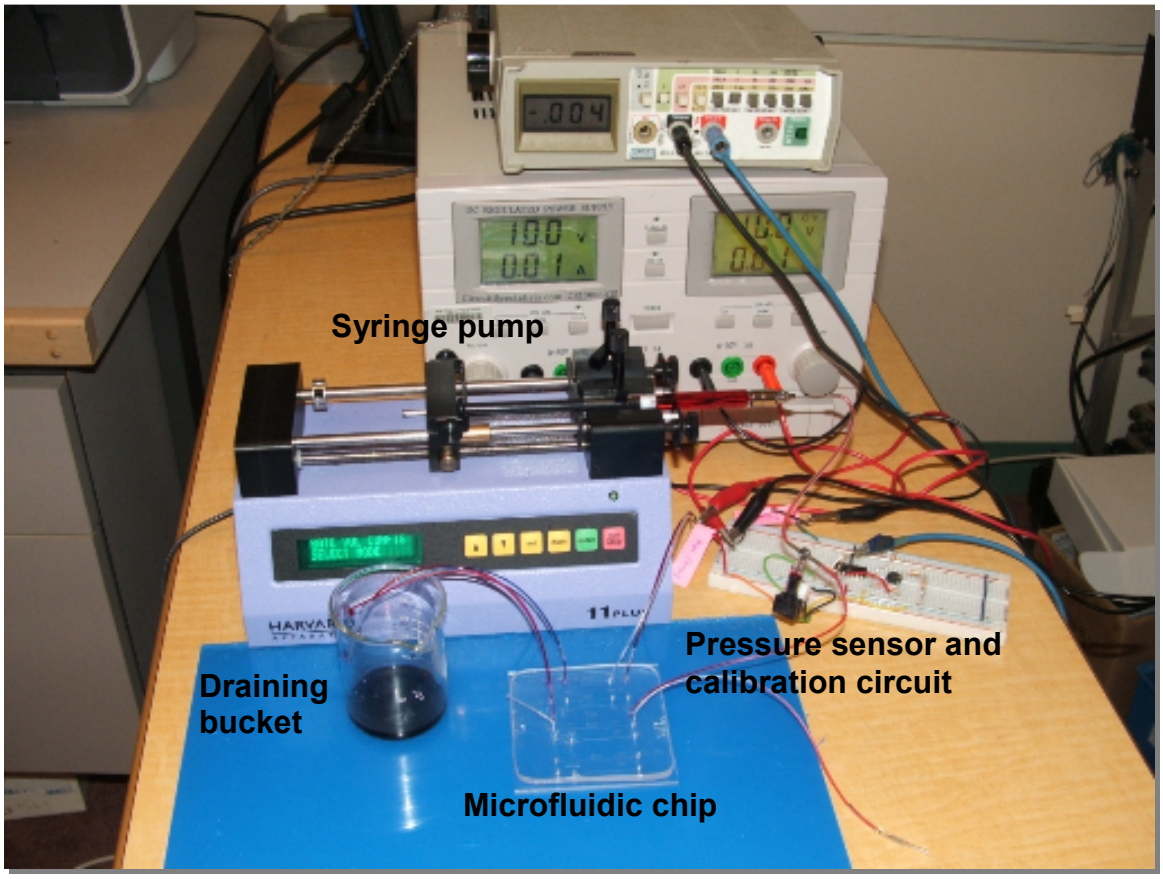

Figure 4-9: Fully assembled system under test.

Red and blue dyed water was run through the channels to examine the flow and to check for leaks. The liquid flow through the channels was increased gradually from 1 to 2 mL/min, which was the maximum rate provided by the Harvard syringe pump 11. At the maximum flow rate, the measured pressure was 68 kPa (note that this number is beyond the maximum rated value of the pressure sensor). Figure 4.10 shows a close-up of the microfluidic chip with an inset of the tube attachment.

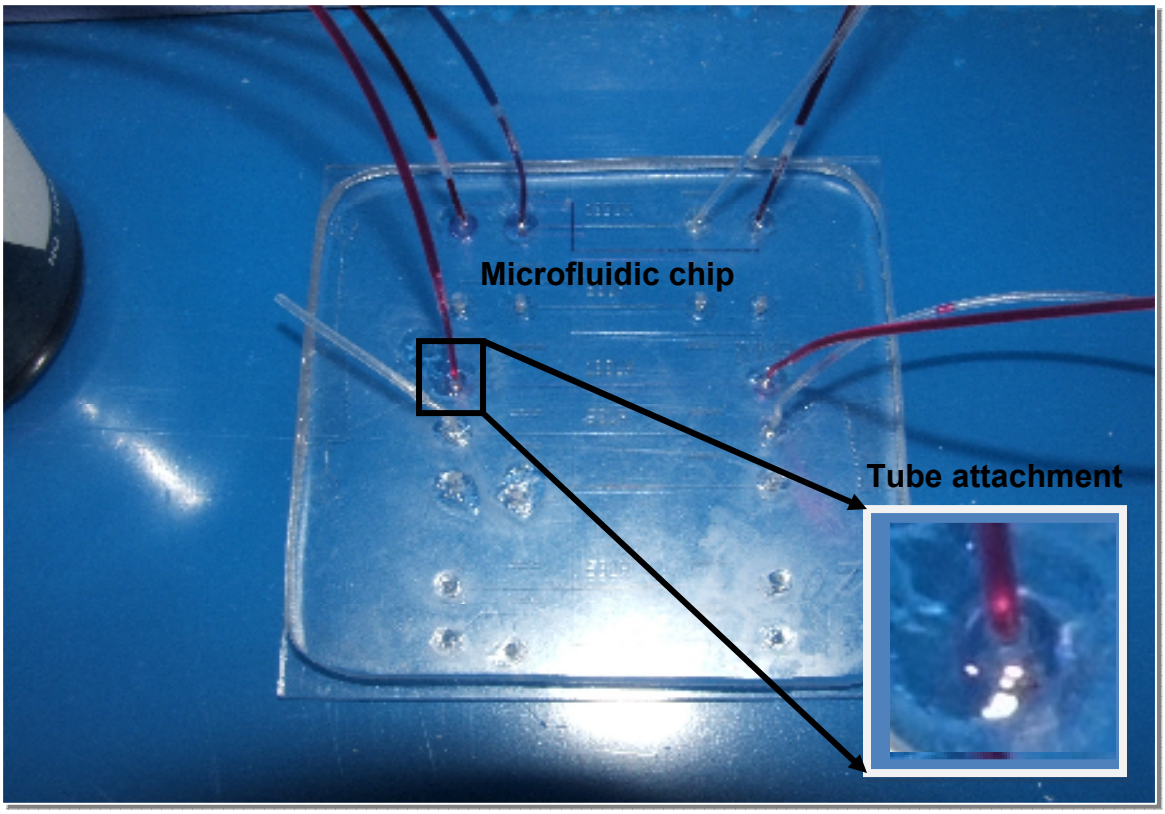

Figure 4-10: Close-up of the microfluidic chip under test with inset of tube attachment.

While running the system at maximum flow and pressure, no leakage was observed for the bonded samples. Figure 4.11 shows the channel under test and a close-up of it. Further, appendix K provides a sequence of pictures taken

during the test, featuring the laminar flow of the red and blue coloured water through the microchannels.

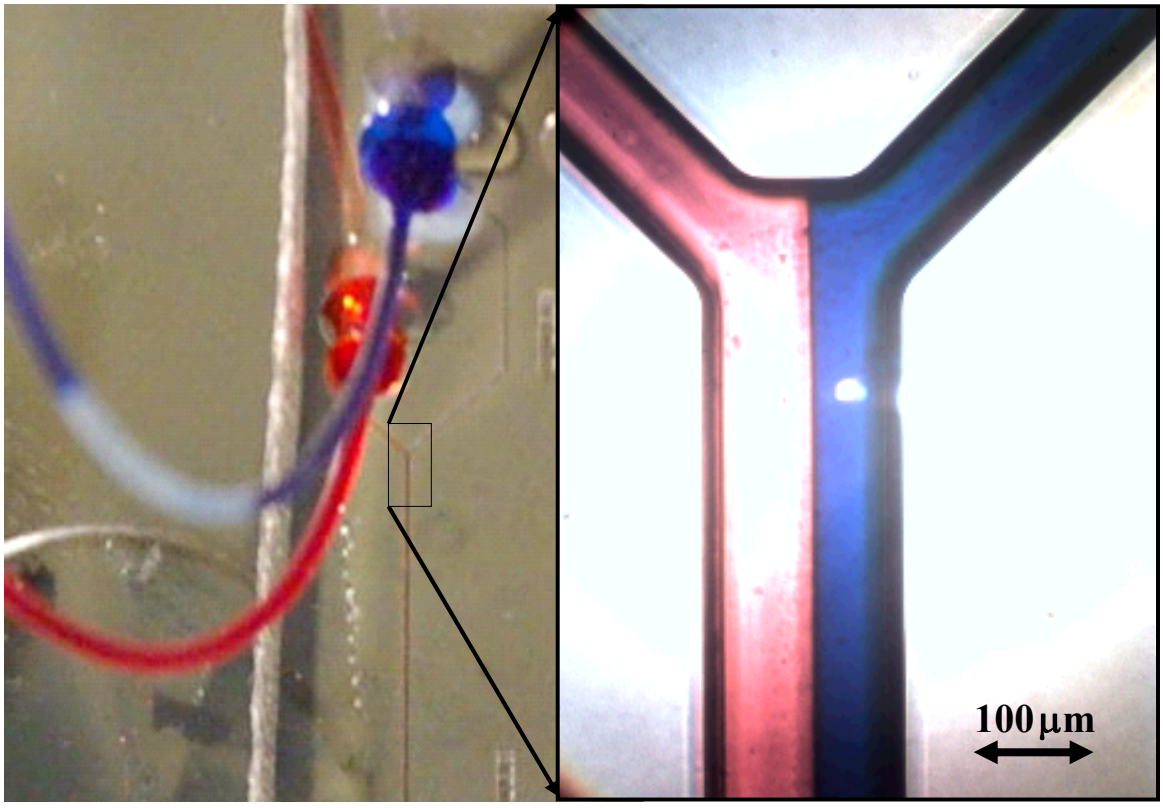

Figure 4-11: A "Y" channel under test (left) and a close-up of the liquid flow (right).

5 PROCESS IMPROVEMENTS

Although the costs associated with the process described are low, the lengthy exposure times increases the process duration considerably. Fabrication of microchannels over 100 μm deep implies exposure times in the order of 30-45 hours. This increased time is partially offset by the number of substrates that can be irradiated simultaneously by scaling the throughput out. Scaling out is a viable option, considering the low cost of the Stratalinker 2400. However, moving to a higher power deep-UV source has the potential of reducing the exposure time. This issue is addressed in the first part of this chapter.

The discussion in section 4.3 pointed out an inevitable drawback of the un-collimated deep-UV, namely negative sidewalls. Having a collimated source would improve considerably the geometry of the channels, allowing for even higher aspect-ratio, LIGA-like, features. Consequently, it would be extremely advantageous to find a way to collimate, if not at least semi-collimate, the radiation. This issue is the subject of the subsequent section of this chapter.

Although reservoirs and microchannels represent the common denominator of almost all μTAS or LOC systems, thermal bonding does not satisfy all their possible geometrical configuration requirements. Addressing an

answer to this problem, a novel bonding method is proposed in the final part of this chapter.

5.1 In-house Built Irradiation Source

All measurements reported in the literature indicate that the absorptivity of PMMA is appreciably low at wavelengths longer than 240 nm [13, 23]. Even at its maximum reported sensitivity [110], which happens at 220 nm, pure PMMA requires doses in excess of 250 mJ/cm^3.

As described in section 4.1, to induce enough chemical change in the OPTIX® PMMA for realizing a 100-μm-deep-channel, a dose in excess of 900 J/cm^2 is required. The power density that the Stratalinker is able to provide is only 4 mW/cm^2. Consequently, exposure times of 60 hours are needed. By increasing the source power, the processing time can be reduced significantly, without sacrificing the quality.

Using the same type of source (i.e., germicidal lamps), the power increase can be achieved in three possible ways:

- by using lamps of a higher power rating;
- by increasing the number of bulbs that are irradiating the same surface;
- by lowering the distance between the bulbs and the substrates.

Focusing mainly on the first two modalities for increasing the power, another irradiation source was built in-house. Photographs of this new irradiation system are shown in figures 5-1 and 5-2.

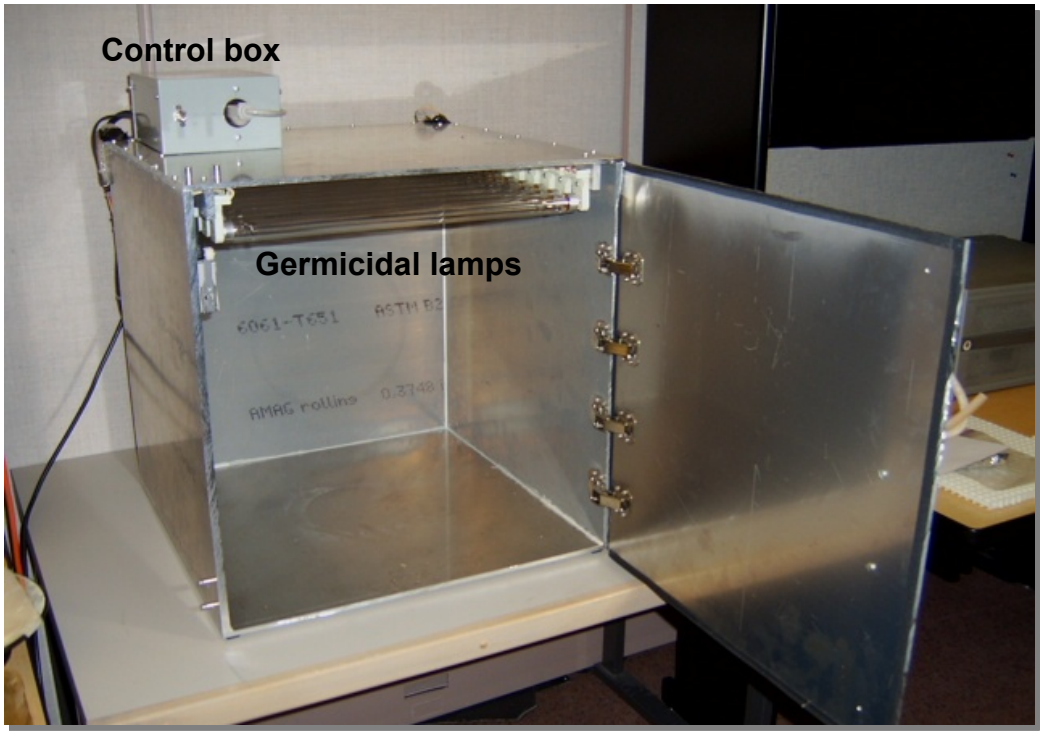

Figure 5-1: The in-house built irradiation box: front view.

Figure 5-2: The in-house built irradiation box: rear view

The number of germicidal lamps was raised to 12 and the lamp power was increased to 25 Watts (as opposed to 5 and 15, respectively, as they were for the Stratalinker).

A cube shaped box with a side of 21" (53.34 cm) made of ¼" (0.635 cm) thick aluminium sheets was constructed. The box is equipped with a safety switch that shuts off the power to the lamps when the door is open. A 20×15×9 cm control box on top of the cube houses a direct current (DC) power supply. This source powers the electronic circuit that drives a relay responsible to close the feeding path for the ballasts, which, in turn, feed the germicidal lamps (see appendix L). A commercial appliance power timer was used to automate the exposure. A manual bypass was incorporated to override the timer for complete manual operation.

A UV photo-detector[12] was employed to measure and verify the deep-UV power levels at different locations inside the newly constructed box as well as the Stratalinker. The measurements confirmed the power levels of 4 mW/cm^2 inside the Stratalinker, whereas, for the same sample distance from the lamps in the newly constructed box, the power density levels were elevated to 11.3 mW/cm^2.

The measurement circuit (see appendix N) consisted of a transimpedance amplifier followed by another amplification stage. The bias was calculated so that the circuit converted a photocurrent of 1nA to an output voltage of 100 mV

[12] The UV sensor is a Schottky-type photodiode on aluminium gallium nitride based material. It operates in a photovoltaic mode. It features good visible blindness and low dark current. Its ratings and characteristics are listed in appendix M.

(i.e., a total gain of 100 mV/nA = 10^8 V/A). The transimpedance amplifier was designed to have a gain of 10^7 V/A and the second amplifier boosts the signal by another factor of 10.

5.2 Light Semi-collimation

Negative sidewall were observed in the fabricated samples due to illumination of the deep-UV source not being perpendicular to the sample surface. To alleviate this problem, a 13 mm thick, honeycomb-like grate, made of 12.5 by 12.5 mm squares, was placed between the bulbs and the substrates. This grate allows only the normal rays from the source to pass through and absorbs rays that emerge at larger angles from the source. The distance between the substrates and the bottom plane of the grate is set to 2 cm. With the grate in place and considering the light coming from a point source situated at 30 cm above the substrates, it hits the substrate surface at angles less than 46 degrees relative to the normal.

Further, to even-out the irradiation so that no square patterns (due to the shadow of the grate) are formed as a result of positioning the grate above the substrates, the samples were set on top of a rotational stage driven by a DC motor operated by a 9 Volt battery. The rotational rate of the stage was approximately 7.5 revolutions per minute. Figure 5-3 shows the rotational stage and the entire assembly is shown in figure 5-4.

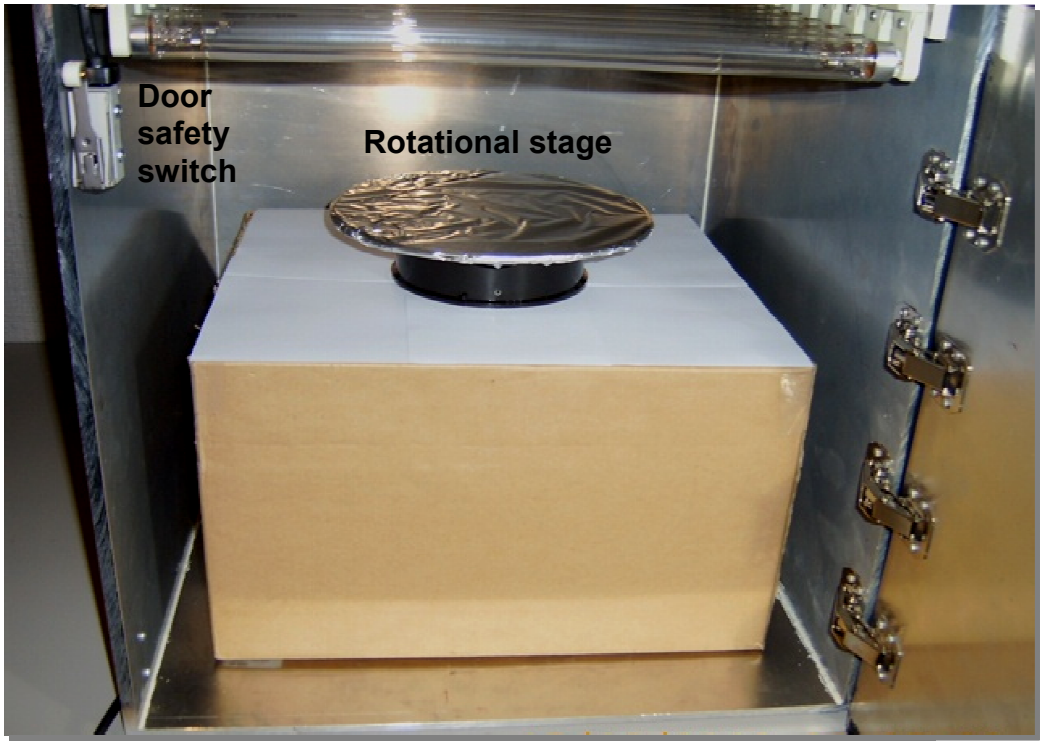

Figure 5-3: The new irradiation box with the rotational stage.

Figure 5-4: The new irradiation box with the rotational stage over which a plastic grate was set in order to semi-collimate the light.

5.3 Adhesion/Bonding of Microfluidic Devices

PMMA is a linear amorphous thermoplastic polymer made of hydrocarbons with an additional atomic component (oxygen). As such, it exhibits low surface energy, tending to be hydrophobic. This property is a limiting factor on the strength of bonds that could be formed between mating surfaces. Not only for PMMA, but also for thermoplastic polymers in general, a variety of approaches have been reported that aim to increase the surface energy, including acid or solvent treatments [151], vacuum [152] and atmospheric [153] plasmas, and surface grafting [154, 155]. However, most of them, if not all, use either expensive equipment or toxic substances.

We have devised a thermal bonding procedure, as presented in section 3.3 that is able to preserve the exceptional optical properties of PMMA as well as retain the compatibility and homogeneity of the channel walls. This method, however, has limitations for low aspect ratio microchannels. In spite of the compressing force being relatively small, the inherent deformation of the channels due to the applied pressure during bonding can be significant with respect to their dimensions. To counteract this deformation, a novel bonding method was developed, which is described below.

The experiments were performed on blank PMMA pieces that were designated to serve as lids for their patterned counterparts. After a cleaning procedure as described in section 3.3, 950 kDa PMMA was spun on top of the substrate for 30 seconds, at 4,000 rpm. This formed a 1.5-2.0 μm layer of liquid

PMMA, which acted as an adhesive in this bonding procedure. The patterned substrate and the lid were then brought into contact, applying only slight pressure by hand. Spreading of the interfacial PMMA liquid on the surface of the patterned surface was easily noticeable, providing the user with a good indication of the areas that were not yet in contact. The substrates were then transferred into a pre-heated (75 °C) oven for 30 min. Molecular entanglement, and hence bonding, is promoted by the anisole content of the liquid PMMA and the temperature in the oven through mechanical interlocking due to diffusion between surfaces. In this type of bonding, a high interfacial compatibility is present, promoting intermixing of polymer chains. Figure 5.5 shows a microfluidic chip bonded using this method. The photograph clearly shows the preservation of transparency of the samples after bonding.

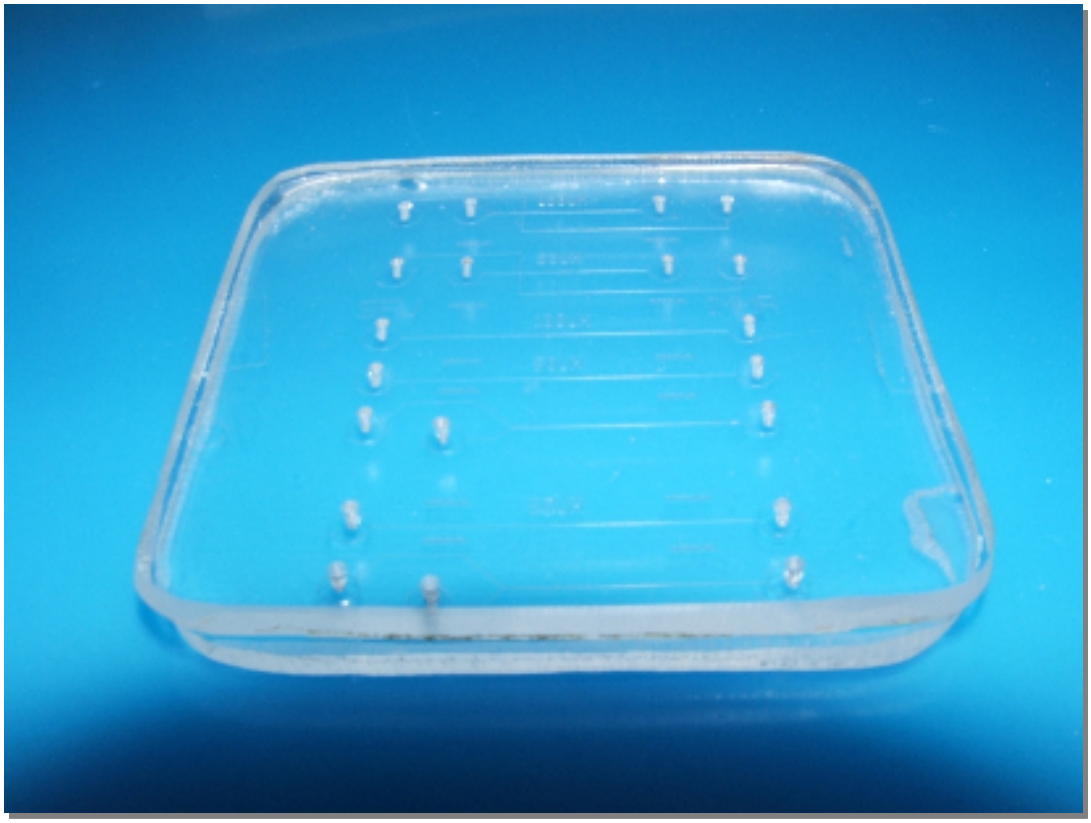

Figure 5-5: Microfluidic chip bonded using an intermediary layer of 950 kDa PMMA.

6 SUMMARY

The work described in this thesis demonstrates the feasibility of patterning inexpensive commercial PMMA using a 254 nm radiation source for manufacturing microfluidic devices. The process uses a relatively inexpensive deep-UV source, which, despite the lengthy exposure times, can expose areas up to 1500 cm^2 in size. PMMA channels can be thermally bonded at low pressure to an unpatterned PMMA sheet to form a complete microfluidic system. Interconnection is easily achieved by direct drilling of holes in the PMMA substrates and attaching PTFE tubing.

The complete process is attractive because it provides inexpensive direct patterning of PMMA microfluidics, can handle very large substrates and allows for easy microfluidic interconnections.

6.1 Future Work

Our process relies on and uses inexpensive resources. However, further optimization would lower the costs and improve the quality of the devices. One modality of reducing costs is avoiding Au deposition on the substrate because this step is the most expensive in the current process. Instead, one of many photoresists that exhibit high deep-UV absorbtion and are resistant to the

radiation damage could be used (e.g., SU-8[13], PMGI[14], etc.). From the same perspective, for mass production, a hard metal mask can be directly placed on top of the substrate during the exposure, thereby reducing the number of process steps.

When the microfluidic chip dimensional features are more than 50 μm in size, a more aggressive developer could be used instead of the co-solvent IPA/water. Recent trials with SU-8 developer[15] were successful in demonstrating elevated dissolution rates. Further, the development could be performed at room temperature.

Another optimization of the process is related to exposure. The germicidal tubes are micro-thin coated inside to filter out unwanted spectrum. However, a distinctive ozone odour is present even after short exposure times, which indicates the presence of 185 nm in the irradiation spectrum. Mainly, this wavelength is responsible for breaking apart the oxygen molecules and creating ozone inside the irradiation box. The ozone creates a shield above the substrates, decreasing the power density of the illumination in time. This phenomenon was noted using the UV sensor circuitry described in section 5.1. To counteract this phenomenon, air can be force-circulated inside the box. Alternatively, the exposure could be performed in vacuum. Both approaches would bring about better process control.

[13] SU-8 is a negative, epoxy-based, near-UV photoresist.
[14] Poly(methylglutarimide) (PMGI) is a positive tone resist, sensitive to deep-UV.
[15] Propylene glycol methyl ether acetate (PGMEA).

6.2 Conclusions

The fabrication procedure outlined throughout this thesis has a number of advantages over other microfluidics processes discussed in the literature [42, 43, 47-54]. First, it uses low-cost materials and an inexpensive exposure system. Second, it is simple, requiring a single mask and a few processing steps. Third, the process is parallel in nature and can be scaled out for producing microfluidic channels on substrates over 900 cm^2 in size. Finally, this process is very safe and environmentally friendly, using relatively non-toxic materials and developers.

APPENDICES

Appendix A: Letter from Dr. Ian Forbes, publisher with the Journal of Micromechanics and Microengineering

SFU Connect Collaboration Suite mhaiducu@sfu.ca

Journal of Micromechanics and Microengineering
Highlights of 2008
Monday, March 02, 2009
4:05:29 PM

From: jmm@iop.org
To: mhaiducu@sfu.ca
Reply To: reply-a.0-c.0-i.0-r.5313@herald.iop.org

Dear Dr Haiducu

I am writing to let you know that Journal of Micromechanics and Microengineering (JMM) has just released the Highlights of 2008, a selection of articles chosen by the Editorial Board and publishing team that best represent the high quality and breadth of the contributions published in the journal last year.

I am delighted to tell you that your paper 'Deep-UV patterning of commercial grade PMMA for low-cost, large-scale microfluidics' has been selected to be part of the Highlights of 2008, and can be found at http://herald.iop.org/jmmbo2008/m137/hxp//link/2380

This special collection will be promoted widely throughout the year and, as part of our website promotion, we are using an electronic banner to encourage people to read the collection. If you and your institution would like to use this banner on your departmental webpage, we would be happy to supply the banner and the link.

You can download the banner at http://herald.iop.org/jmmbannerred/m137/hxp//deliver /JMM(468x60)NovRED.gif and the link to the webpage is http://herald.iop.org/jmmbo2008 /m137/hxp//link/2380

Once again, congratulations.

Best wishes,
Dr Ian Forbes
Publisher
Journal of Micromechanics and Microengineering
jmm@iop.org
www.iop.org/journals/jmm

Data Protection
The Institute of Physics (and other companies in its group, including IOP Publishing Limited) may like to send you further notifications like this. If you would prefer not to receive these, then please reply to this e-mail with the word "unsubscribe" in the subject line. We will never rent or sell your e-mail address to any third parties.
Zimbra: mhaiducu@sfu.ca https://connect.sfu.ca/zimbra/mail
1 of 1 5/3/2009 1:09 PM

Appendix B: OPTIX® and GoodFellow CQ Grade Acrylic Sheet Properties

Table B-1: OPTIX® acrylic sheet properties [140].

Physical Properties	Units	Values
Specific Gravity	-	1.19
Optical Refractive Index	-	1.49
Light Transmittance (Total / Haze)	%	92/2
Water Absorption	% by weight	0.40
Shrinkage	%	<5%
Mechanical Properties	**Units**	**Values**
Tensile Strength – Max.	psi	11,030
Tensile Elongation – Max.	%	5.8
Tensile / Flexural Modulus of Elasticity	psi	490,000
Flexural Strength	psi	17,000
Thermal Properties	**Units**	**Values**
Softening Temperature	°C	99 - 104
Coefficient of Thermal Expansion (-30 to +300°C)	$[in/(in \cdot °F)] \cdot 10^{-5}$	3.0

Table B-2: GoodFellow CQ grade acrylic sheet properties [143].

Physical Properties	Units	Values
Density	g/cm^3	1.19
Limiting oxygen index	%	17 - 20
Refractive index	-	1.49
Resistance to UV	-	good
Water absorption (over 24 h)	%	0.2
Mechanical Properties	**Units**	**Values**
Hardness – Rockwell	-	M92 - 100
Poisson's Ratio	-	0.35 - 0.40
Tensile modulus	GPa	2.4 - 3.3
Tensile strength	MPa	80
Thermal Properties	**Units**	**Values**
Coefficient of thermal expansion ($\times 10^{-6} K^{-1}$)	-	70 - 77
Specific heat	J/(K×Kg)	1400 - 1500
Thermal conductivity	W/(m×K)	0.17 - 0.19 @23°C

Appendix C: Acrylite® OP-4 Acrylic Sheet Properties

Table C-1: Acrylite® OP-4 acrylic sheet properties [144].

Physical Properties	Units	Values
Specific Gravity	-	1.19
Optical Refractive Index	-	1.49
Light Transmission, Total	-	92%
Water Absorption (over 24h)	24 hrs @ 73°F	0.2%
Water Absorption (long term)	7 days	0.5%
Mechanical Properties	**Units**	**Values**
Tensile Strength	MPa	69
Flexural Strength	MPa	114
Modulus of Elasticity (Elongation)	MPA	2,800
Modulus of Elasticity (Flexural)	MPa	3,300
Rockwell Hardness	-	M94
Thermal Properties	**Units**	**Values**
Coefficient of Linear Thermal Expansion ($10^{-6}K^{-1}$)	in/in/°F	0.00004
Specific Heat @ 77°F	J/kg×K	1470
Coefficient of Thermal Conductivity (k-Factor)	w/mK	0.19
Electrical Properties	**Units**	**Values**
Dielectric Constant	@60Hz/1KHz	3.5/3.2
Dielectric Strength	Volts/mil	430
Surface Resistivity	Ohms	1.9×10^{15}
Volume Resistivity	Ohms×cm	1.6×10^{16}

Appendix D: Absorption Measurements for UVT OP-4, OPTIX®, and PMMA 495kDa

Table D-1: Direct (i.e., not normalized for thickness) absorption readings in cm^{-1} taken with Cary 300 Bio UV-visible spectrophotomer.

Substrate ↓	Dose (J/cm^2) →	0	72	144	216	288	360
UVT		2.19	3.33	3.27	3.50	3.61	3.59
OPTIX®		4.33	4.90	5.10	4.88	4.91	6.13
PMMA 495		1.10	3.32	3.66	3.80	3.82	4.60

Table D-2: Absolute absorbance values for UVT OP-4, OPTIX®, and PMMA 495 kDa.

Substrate ↓	Dose (J/cm^2) →	0	72	144	216	288	360
UVT		117.70	179.26	185.00	199.65	207.24	211.34
OPTIX®		101.07	110.14	112.31	112.25	113.94	114.38
PMMA 495		102.85	187.59	194.60	196.44	201.21	221.21

Appendix E: PMMA Patterning Process Recipe

Table E-1: PMMA patterning process recipe.

Sample PMMA 3X3”	Parameter	Time	Notes
Clean w/ DI water & soap, followed by N_2 dry		10 min	
Clean w/ methanol (CH_3OH) followed by N_2 dry			
Deposit 100 nm of Au @ 80W			
Spin S1813 resist	4000 rpm	30 s	
Bake HP	75°C	3 min	Tape test (optional)
Expose		10 s	
Develop MF-319	RT[16]	1 min	
Rinse DI, followed by N_2 dry		30 s	
Microscopy w/ yellow filter			Check for underdevelopment
Etch Au	RT	30 s	
Rinse DI, followed by N_2 dry		30 s	
Microscopy w/ yellow filter			Check for bloating, over/under etch
Expose (Flood)		60 s	
Develop MF-319	RT	30 s	
Rinse DI, followed by N_2 dry		30 s	
Profilometry (Au to PMMA)[17]			(optional) Au thickness:
Deep UV Radiation	RT	900 min	
Etch irradiated PMMA[18]	28°C	1 hour	
Clean w/ acetic acid (CH_3COOH)	RT	30 s	
Rinse DI, followed by N_2 dry		30 s	
Profilometry (PMMA channel depth)[19]			

[16] RT stands for room temperature
[17] Expected thickness is 100 nm
[18] 7:3 IPA (isopropyl alcohol C_3H_8O):H_2O
[19] Expected thickness is approx. 60 μm

Appendix F: Etch Depths of OPTIX® PMMA Exposed with Multiple Doses of 216 J/cm^2 of Deep-UV Radiation

Table F-1: Etch depths of OPTIX® PMMA (development without agitation).

Exposure Dose (J/cm^2) ↓	Development Time (minutes) →	0	10	20	30	40	50	60
216	Depth_1	0.00	12.11	27.51	34.87	40.38	48.24	53.18
	Depth_2	0.00	10.03	24.66	31.25	39.46	44.81	50.04
	Depth_3	0.00	7.50	19.93	24.88	32.32	36.88	41.05
	Depth_4	0.00	9.16	23.13	29.41	37.47	43.4	43.33
	Average	**0.00**	**9.70**	**23.81**	**30.10**	**37.41**	**43.33**	**46.90**
432	Depth_1	0.00	42.85	65.19	73.57	83.78	87.74	92.32
	Depth_2	0.00	42.53	65.94	73.93	83.99	87.95	92.59
	Depth_3	0.00	43.45	66.61	74.65	83.95	86.79	92.89
	Depth_4	0.00	41.11	65.82	79.92	83.87	87.52	92.08
	Average	**0.00**	**42.48**	**65.89**	**75.52**	**83.90**	**87.50**	**92.47**
648	Depth_1	0.00	55.37	70.13	81.92	90.36	94.49	97.38
	Depth_2	0.00	54.85	69.70	82.03	89.56	94.25	99.28
	Depth_3	0.00	53.54	66.58	79.80	88.39	92.08	98.30
	Depth_4	0.00	52.34	67.85	78.61	87.95	92.14	98.98
	Average	**0.00**	**54.03**	**68.57**	**80.59**	**89.07**	**93.24**	**98.49**
864	Depth_1	0.00	52.10	73.39	81.53	90.40	95.37	98.72
	Depth_2	0.00	51.59	73.01	81.76	89.40	94.46	97.79
	Depth_3	0.00	52.96	73.17	82.99	91.14	96.56	99.11
	Depth_4	0.00	52.06	73.13	81.56	91.56	96.51	100.20
	Average	**0.00**	**52.18**	**73.18**	**81.96**	**90.63**	**95.73**	**98.96**

Appendix G: Etch Depths of UVT OP-4 PMMA Exposed with Multiple Doses of 216 J/cm^2 of Deep-UV Radiation

Table G-1: Etch depths of UVT OP-4 PMMA (development without agitation).

Exposure Dose (J/cm^2) ↓	**Development Time (minutes) →**	**0**	**10**	**20**	**30**	**40**	**50**	**60**
216	Depth_1	0.00	47.01	73.15	86.40	107.60	106.00	128.20
	Depth_2	0.00	50.02	65.60	97.40	106.40	114.60	121.50
	Depth_3	0.00	55.00	72.80	83.60	95.60	119.80	125.80
	Depth_4	0.00	50.03	77.80	87.89	99.00	114.70	120.50
	Average	**0.00**	**50.52**	**72.33**	**88.82**	**102.15**	**113.77**	**124.00**
432	Depth_1	0.00	73.00	119.00	143.00	155.00	179.00	182.00
	Depth_2	0.00	79.90	121.00	142.00	157.00	175.00	189.00
	Depth_3	0.00	85.50	122.00	140.00	164.00	175.00	185.40
	Depth_4	0.00	80.19	120.90	145.60	166.00	178.00	186.50
	Average	**0.00**	**79.64**	**120.72**	**142.65**	**160.50**	**176.75**	**185.72**
648	Depth_1	0.00	86.70	123.00	142.40	165.00	OOR[20]	OOR
	Depth_2	0.00	96.70	116.00	146.80	161.00	OOR	OOR
	Depth_3	0.00	82.00	119.00	134.60	154.00	OOR	OOR
	Depth_4	0.00	101.00	120.70	146.40	157.00	OOR	OOR
	Average	**0.00**	**91.60**	**119.67**	**142.55**	**159.25**	OOR	OOR
864	Depth_1	0.00	90.10	133.70	150.00	161.00	OOR	OOR
	Depth_2	0.00	86.00	134.00	138.00	160.70	OOR	OOR
	Depth_3	0.00	85.60	131.00	150.40	166.70	OOR	OOR
	Depth_4	0.00	85.60	130.00	144.00	161.60	OOR	OOR
	Average	**0.00**	**86.82**	**132.17**	**145.60**	**162.50**	OOR	OOR

[20] OOR stands for out of range. The measurement could not be taken for it was out of the measurable range of our profilometer

Appendix H: Etch Depths of OPTIX® PMMA Exposed Through a 5 nm Thick Titanium Barrier Layer with Multiple Doses of 216 J/cm^2 of Deep-UV Radiation

Table H-1: Etch depths of OPTIX® PMMA exposed through a 5 nm thick Ti barrier layer.

Exposure Dose (J/cm^2) ↓	Development Time (minutes) →	0	10	20	30	40	50	60
216	Depth_1	0.00	38.95	52.87	62.06	68.90	77.52	86.60
	Depth_2	0.00	37.70	51.76	61.12	69.90	78.69	82.82
	Depth_3	0.00	38.83	53.67	62.87	68.59	77.18	81.24
	Depth_4	0.00	38.99	54.14	63.81	66.71	75.64	80.64
	Average	**0.00**	**38.62**	**53.11**	**62.46**	**68.52**	**77.28**	**81.83**
432	Depth_1	0.00	45.92	64.04	77.22	84.80	92.15	98.88
	Depth_2	0.00	46.38	65.22	78.40	85.24	93.06	97.24
	Depth_3	0.00	43.22	62.03	75.61	81.53	89.46	92.42
	Depth_4	0.00	42.42	60.85	75.69	80.89	88.88	93.14
	Average	**0.00**	**44.48**	**63.03**	**76.73**	**83.12**	**90.88**	**95.42**
648	Depth_1	0.00	61.22	84.34	89.34	98.58	103.9	108.20
	Depth_2	0.00	59.00	83.89	89.08	98.68	103.7	108.60
	Depth_3	0.00	62.95	80.47	91.97	101.50	106.00	111.60
	Depth_4	0.00	57.79	80.73	90.36	100.20	105.30	111.00
	Average	**0.00**	**60.24**	**82.35**	**90.19**	**99.74**	**104.73**	**109.85**
864	Depth_1	0.00	68.97	89.41	101.8	107.60	115.30	118.30
	Depth_2	0.00	65.09	85.07	98.99	104.90	112.10	115.80
	Depth_3	0.00	67.05	86.26	98.34	104.50	112.10	115.30
	Depth_4	0.00	66.32	86.81	99.66	106.20	113.60	116.60
	Average	**0.00**	**66.85**	**86.88**	**99.69**	**105.80**	**113.28**	**116.50**

Appendix I: Etch Depths of OPTIX® PMMA Exposed with Multiple Doses of 216 J/cm^2 of Deep-UV Radiation. Development Performed With Mechanical Agitation

Table I-1: Etch depths of OPTIX® PMMA (development with agitation).

Exposure Dose (J/cm^2) ↓	**Development Time (minutes) →**	**0**	**10**	**20**	**30**	**40**	**50**	**60**
216	Depth_1	0.00	19.78	35.77	41.52	50.63	54.79	59.55
	Depth_2	0.00	14.22	30.11	35.26	42.90	48.41	51.19
	Depth_3	0.00	14.17	29.61	39.31	43.21	47.38	51.18
	Depth_4	0.00	18.87	35.83	43.33	51.80	54.09	59.99
	Average	**0.00**	**16.76**	**35.68**	**39.85**	**47.13**	**51.16**	**55.47**
432	Depth_1	0.00	54.01	70.09	78.15	84.48	89.79	100
	Depth_2	0.00	54.47	70.72	78.45	86.46	92.09	102.54
	Depth_3	0.00	55.52	72.57	81.32	87.96	93.08	103.09
	Depth_4	0.00	54.94	71.83	80.21	88.25	92.19	102.6
	Average	**0.00**	**54.73**	**71.30**	**79.53**	**86.78**	**91.78**	**102.05**
648	Depth_1	0.00	73.35	86.92	99.61	105.00	113.70	116.1
	Depth_2	0.00	75.35	97.99	99.73	105.30	114.50	117.4
	Depth_3	0.00	73.69	86.61	99.41	105.06	112.20	116.1
	Depth_4	0.00	72.25	85.51	98.32	103.8	111.50	115.6
	Average	**0.00**	**73.66**	**86.75**	**99.26**	**104.79**	**112.97**	**116.3**
864	Depth_1	0.00	73.35	91.61	101.4	105.70	114.70	120
	Depth_2	0.00	70.08	88.93	98.52	104.70	112.00	117.8
	Depth_3	0.00	69.44	87.63	97.18	105.50	108.80	116.3
	Depth_4	0.00	73.69	91.54	100.9	109.00	114.80	119.6
	Average	**0.00**	**71.64**	**89.92**	**99.5**	**106.47**	**112.57**	**118.42**

Appendix J: Etch Depths of UVT OP-4 PMMA Exposed with Multiple Doses of 216 J/cm^2 of Deep-UV Radiation. Development Performed With Mechanical Agitation

Table J-1: Etch depths of UVT OP-4 PMMA (development with agitation).

Exposure Dose (J/cm^2) ↓	**Development Time (minutes) →**	**0**	**10**	**20**	**30**	**40**	**50**	**60**
216	Depth_1	0.00	51.90	90.00	107.00	121.30	106.00	128.20
	Depth_2	0.00	51.17	91.40	106.40	123.10	114.60	121.50
	Depth_3	0.00	50.45	90.00	105.80	119.70	119.80	125.80
	Depth_4	0.00	49.13	92.16	104.80	120.80	114.70	120.50
	Average	**0.00**	**50.66**	**90.89**	**106.00**	**121.22**	**113.77**	**124.00**
432	Depth_1	0.00	85.00	126.00	144.00	152.00	179.00	182.00
	Depth_2	0.00	84.00	127.00	145.00	154.00	175.00	189.00
	Depth_3	0.00	94.00	129.00	137.00	159.00	175.00	185.40
	Depth_4	0.00	92.00	131.00	145.00	160.00	178.00	186.50
	Average	**0.00**	**88.75**	**128.25**	**142.75**	**156.25**	**176.75**	**185.72**
648	Depth_1	0.00	108.00	131.60	155.00	OOR[21]	OOR	OOR
	Depth_2	0.00	109.40	131.00	154.10	OOR	OOR	OOR
	Depth_3	0.00	111.00	127.80	157.10	OOR	OOR	OOR
	Depth_4	0.00	106.90	125.70	156.10	OOR	OOR	OOR
	Average	**0.00**	**108.82**	**129.02**	**155.58**	OOR	OOR	OOR
864	Depth_1	0.00	109.00	135.90	155.00	OOR	OOR	OOR
	Depth_2	0.00	111.00	132.00	160.00	OOR	OOR	OOR
	Depth_3	0.00	108.00	134.00	156.00	OOR	OOR	OOR
	Depth_4	0.00	106.00	143.00	155.00	OOR	OOR	OOR
	Average	**0.00**	**108.50**	**136.22**	**156.50**	OOR	OOR	OOR

[21] OOR stands for out of range. The measurement could not be taken for it was out of the measurable range of our profilometer.

Appendix K: Sequence of Pictures Taken During the Microfluidic System Test

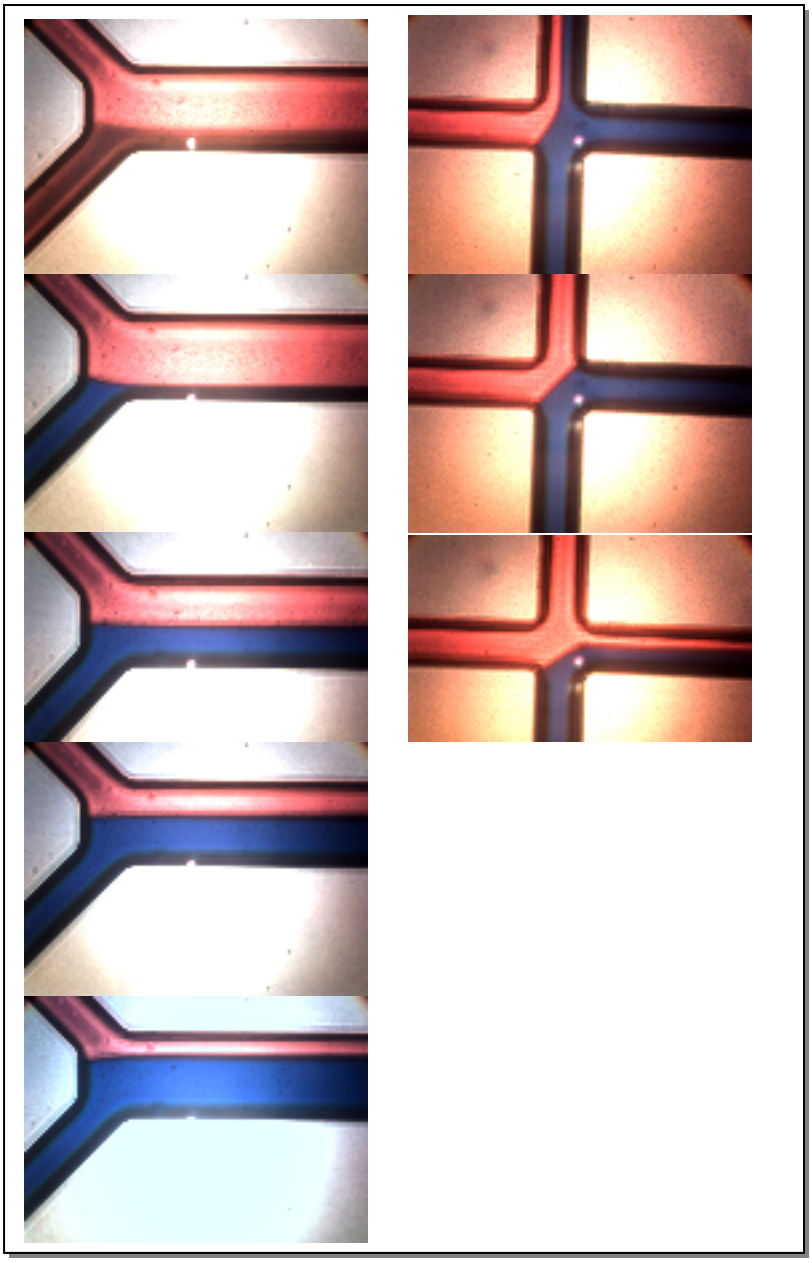

Figure K-1: Snap shots showing the laminar flow of the red and blue colored water through the microchannels. A "Y"- channel is shown on the left and a channel cross on the right.

Appendix L: Power Supply and Control Circuit - Schematic Diagram

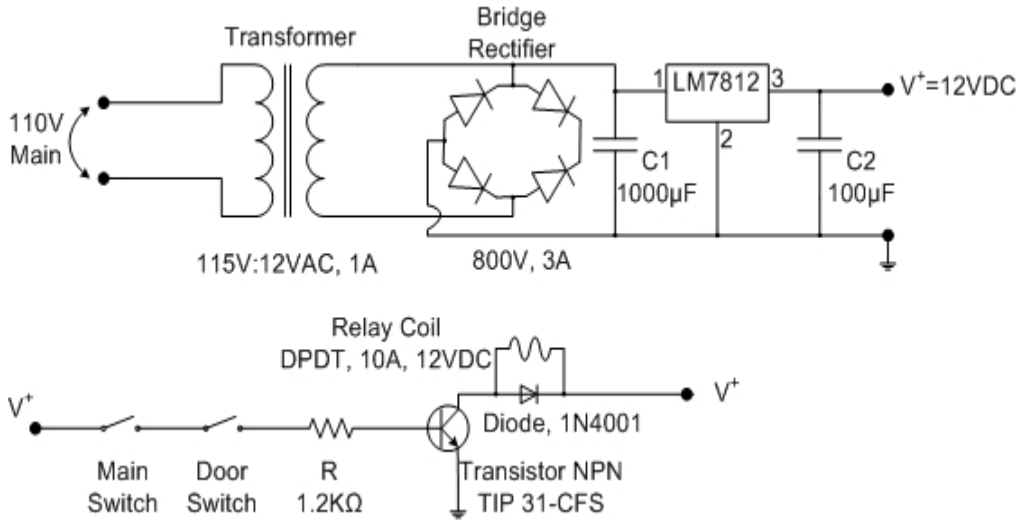

Figure L-1: Schematic diagram of the power supply and the control circuit for the germicidal lamps ballasts.

Appendix M: Photodiode GUVB-T11GD Data Sheet

Table M-1: Absolute maximum ratings for GUVB-T11GD.

Parameter	Symbol	Min.	Max.	Unit	Remark
Storage temperature	Tst	-40	90	°C	
Operating Temperature	Top	-30	85	°C	
Reverse Voltage	Vr, max.		3	V	
Forward Current	If, max.		1	mA	
Soldering Temperature	Tsol		260	°C	Within 10 sec

Table M-2: Characteristics of GUVB-T11GD (at 25°C).

Parameter	Symbol	Min.	Typ.	Max.	Unit	Remark
Dark Current	Id			1	nA	Vr = 0.1V
Photo Current	Iph		51		nA	UVA Lamp, 1mW/cm^2
Temperature Coefficient	Itc		0.05		%/°C	UVA Lamp
Responsivity	R		0.13		A/W	λ = 350nm, Vr = 0V
Spectral Detection Range	λ	220		320	nm	
Breakdown Voltage	V_{BR}		5			Ir = 1 μ A

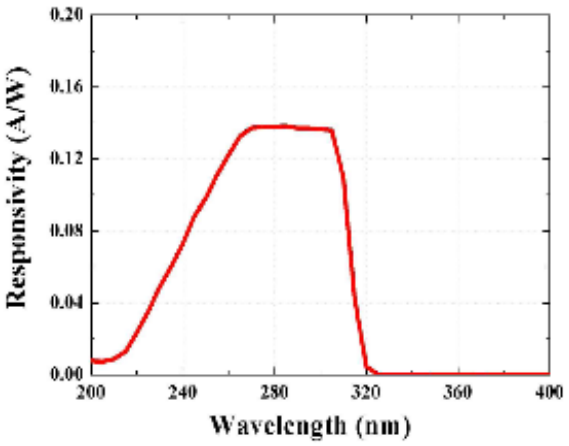

Figure M-1: Responsivity curve of GUVB-T11GD.

Appendix N: Electronic Circuit Used to Measure the Deep-UV Power Levels Inside Stratalinker 2400 and the In-house Built Irradiation Box

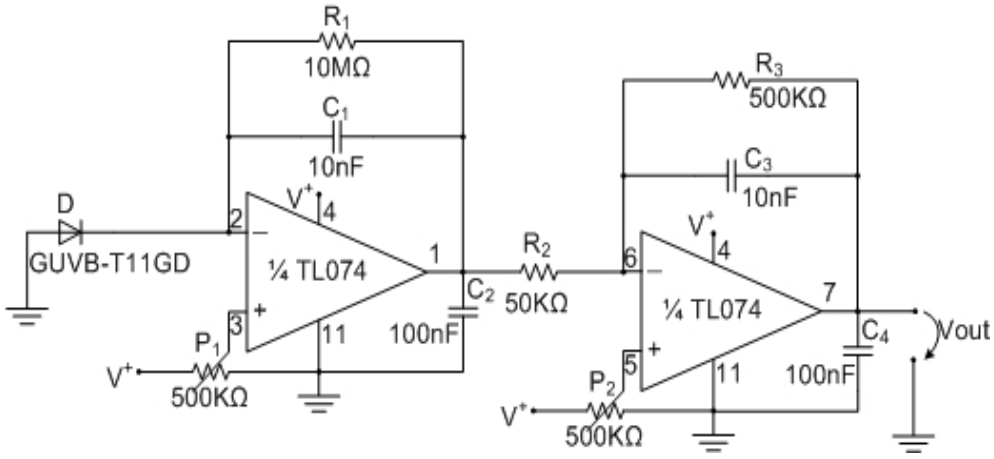

Figure N-1: Schematic diagram of the electronic circuit used to measure the deep-UV power levels.

According to spectral response given in appendix M (fig. M-1), the responsivity of the sensor at 254 nm is 0.09 A/W. Consequently, a UV power of 11.11 mW would generate a photocurrent of 1 nA. Taking into consideration that the sensitivity area of the sensor is 0.076 mm^2, then a photocurrent of 1 nA is generated by a deep-UV power density of 146.1988 nW/mm^2 =

= 14,619.88 $nW/cm^2 \approx 0.015$ mW/cm^2. The circuit above converts a photo-current of 1 nA to a voltage of 100 mV at the output.

Reference List

1. Kopp, M.U., H.J. Crabtree, and A. Manz, *Developments in Technology and Applications of Microsystems.* Current Opinion in Chemical Biology, 1997. **1**(3): p. 410-419.
2. Chen, S.-H. and J.M. Gallo, *Use of Capillary Electrophoresis Methods to Characterize the Pharmacokinetics of Aantisense Drugs.* Electrophoresis, 2005. **19**(16-17): p. 2861-2869.
3. Hicks, J., *Genetics and Drug Discovery Dominate Microarray Research.* Research & Development, 1999. **41**(2): p. 28-33.
4. Jakeway, S.C., A.J.d. Mello, and E.L. Russell, *Miniaturized Total Analysis Systems for Biological Analysis.* Fresenius' Jurnal of Analytical Chemistry, 2000. **366**(6-7): p. 525-539.
5. Schult, K., et al., *Disposable Optical Sensor Chip for Medical Diagnostics: New Ways in Bioanalysis.* Analytical Chemistry, 1999. **71**(23): p. 5430-5435.
6. Wang, J., et al., *DNA Electrochemical Biosensors for Environmental Monitoring. A review.* Analytica Chimica Acta, 1997. **347**(1-2): p. 1-8.
7. Whitesides, G.M., *The Origins and the Future of Microfluidics.* Nature, 2006. **442**: p. 368-373.
8. Bakajin, O.B., et al., *Electrohydrodynamic Stretching of DNA in Confined Environments.* Physical Review Letters, 1998. **80**(12): p. 2737-2740.
9. Turner, S.W.P., M. Cabodi, and H.G. Craighead, *Confinement-Induced Entropic Recoil of Single DNA Molecules in a Nanofluidic Structure.* Physical Review Letters, 2001. **88**(12): p. 128103-1 - 128103-4.
10. Becker, H. and C. Gärtner, *Polymer Microfabrication Methods for Microfluidic Analytical Applications.* Electrophoresis, 2000. **21**(1): p. 12-26.
11. Boone, T.D., et al., *Plastic Advances Microfluidic Devices.* Analytical Chemistry, 2002. **74**(3): p. 78A-86A.
12. Becker, H. and L.E. Locascio, *Polymeric Microfluidic Devices.* Talanta, 2002. **56**(2): p. 267-287.
13. Madou, M.J., *Fundamentals of Microfabrication: The Science of Miniaturization*. 2002: CRC. 752.

14. Johnstone, R., I.G. Foulds, and M. Parameswaran, *Deep-uv exposure of poly(methyl methacrylate) at 254 nm using low-pressure mercury vapour lamps.* Journal of Vacuum Science and Technology B, 2008. **26**(2): p. 682-685.

15. Johnstone, R.W., I.G. Foulds, and M. Parameswaran. *Exposure and Development of Poly (methyl methacrylate) using 254nm Light Source and IPA/Water*. in *Proceedings of the Canadian Conference on Electrical and Computer Engineering (2007). CCECE* 2007. Vancouver, BC, Canada: IEEE.

16. Haiducu, M., et al., *Deep-UV Patterning of Commercial Grade PMMA for Low-Cost, Large-Scale Microfluidics.* Journal of Micromechanics and Microengineering, 2008. **18**(11): p. 115029-115036.

17. Willson, C.G., *Introduction to Microlithography*, in *Introduction to Microlithography (2nd edition)*, L.F. Thompson, C.G. Willson, and M.J. Bowden, Editors. 1994, American Chemical Society: Washington, D.C. p. 123.

18. *Stratalinker uv crosslinker: Instruction manual.* http://www.stratagene.com/manuals/7003406.pdf.

19. Manz, A., N. Graber, and H.M. Widmer, *Miniaturized total chemical analysis systems: a novel concept for chemical sensing.* Sensors and Actuators B: Chemical, 1990. **1**: p. 244-248.

20. Manz, A., et al., *Planar Chips Technology for Miniaturization and Integration of Separation Techniques into Monitoring Systems. Capillary Electrophoresis on a Chip.* Journal of Chromatography A, 1992. **593**(1-2): p. 253-258.

21. Harrison, D.J., et al., *Capillary Electrophoresis and Sample Injection Systems Integrated on a Planar Glass Chip.* Analytical Chemistry, 1992. **64**(17): p. 1926-1932.

22. Terry, S.C., J.H. Jerman, and J. Angell, *A Gas Chromatographic Air Analyzer Fabricated on a Silicon Wafer.* IEEE Transaction on Electron Devices, 1979. **26**(12): p. 1880-1886.

23. Moreau, W.M., *Semiconductor Lithography: Principles, Practices, and Materials*. 1987, New York: Plenum Publishing Corporation. 952.

24. Thompson, L.F., C.G. Willson, and M.J. Bowden, *Introduction to Microlithography*. 1994, Washington, DC: American Chemical Society.

25. Sze, S.M., *Semiconductor Devices: Physics and Technology*. 1983, New York: John Wiley & Sons.

26. Robbins, H.R. and B. Schwartz, *Chemical Etching of Silicon - I. The System, HF, HNO_3 and H_2O.* Journal of Electrochemical Society, 1959. **106**: p. 505-508.

27. Robbins, H.R. and B. Schwartz, *Chemical Etching of Silicon - II. The System HF, HNO_3, H_2O, and $HC_2C_3O_2$.* Journal of Electrochemical Society, 1960. **107**(108-111).

28. Schwartz, B. and H.R. Robbins, *Chemical Etching of Silicon - III. A Temperature Study in the Acid System.* Journal of Electrochemical Society, 1961. **108**: p. 365-372.

29. Schwartz, B. and H.R. Robbins, *Chemical Etching of Silicon - IV. Etching Technology.* Journal of Electrochemical Society, 1976. **123**: p. 1903-1909.

30. Kern, W. and C.A. Deckert, *Chemical Etching*, in *Thin Film Processes*, J.L. Vossen and W. Kern, Editors. 1978, Academic Press: Orlando, CA.

31. Lehman, H.W., *Plasma-Assisted Etching*, in *Thin Film Processes II*, J.L. Vossen and W. Kern, Editors. 1991, Academic Press: Boston, MA. p. 673-748.

32. Nguyen, N.-T. and S.T. Wereley, *Fundamentals and Applications of Microfluidics*. 2002: Artech House. 471.

33. Stoller, A.I., *The Etching of Deep Vertical-Walled Patterns in Silicon.* RCA Review, 1970. **31**(2): p. 271-275.

34. Holland, L., *Thin Film Microelectronics*. 1965, London: Chapman and Hall

35. Kovacs, G.T.A., K. Petersen, and M. Albin, *Silicon Micromachining - Sensors to Systems.* Analytical Chemistry, 1996. **68**(13): p. A407-A412.

36. Harrison, D.J., et al., *Micromachining a Miniaturized Capillary Electrophoresis-based Chemical Analysis System On a Chip.* Science, 1993. **261**: p. 895-897.

37. Harrison, D.J., P.G. Glavina, and A. Manz, *Towards Miniaturized Electrophoresis and Chemical Analysis Systems on Silicon: An Alternative to Chemical Sensors.* Sensors and Actuators B: Chemical, 1993. **10**(2): p. 107-116.

38. Jeong, Y., et al., *Methodology for Miniaturized CE and Insulation on a Silicon Substrate* Lab on a Chip, 2001. **1**(2): p. 143-147.

39. Mello, A.d., *Plastic Fantastic.* Lab on a Chip, 2002. **2**(2): p. 31-36.

40. Fan, Z.H. and A.J. Ricco, *Plastic Microfluidic Devices for DNA and Protein Analyses* in *BioMEMS and Biomedical Nanotechnology.* , M. Ferrari, M. Ozkan, and M.J. Heller, Editors. 2007, Springer US.

41. VerLee, D., et al. *Fluid Circuit Technology: Integrated Interconnect Technology for Microfluidic Devices*. in *IEEE Solid-State Sensor and Actuator Workshop*. 1996.

42. Becker, H., W. Dietz, and P. Dannberg. *Microfluidic Manifolds by Polymer Hot Embossing for µ-TAS Applications*. in *MicroTotal Analysis Systems '98*. 1998. Banff, Canada.

43. Locascio, L.E., et al. *Plastic Microfluid Devices for Clinical Measurements*. in *MicroTotal Analysis Sstems '98*. 1998. Banff, Canada.

44. McCormick, R.M., et al., *Microchannel electrophoretic separations of DNA in injection-molded plastic substrates.* Analytical Chemistry, 1997. **69**: p. 2626-2630.

45. Locascio, L.E., et al., *Fabrication of Polymer Microfluidic Systems by Hot Embossing and Laser Ablation*, in *Microchip Capillary Electrophoresis: Methods and Protocols*, C.S. Henry, Editor. 2006, Springer. p. 37-46.

46. Martynova, L., et al., *Fabrication of plastic microfluid channels by imprinting methods.* Analytical Chemistry, 1997. **69**: p. 4783-4789.

47. Ekstrand, G., et al., *Integrated Cell Based Assays in Microfabricated Disposable CD Devices*, in *MicroTotal Analysis Systems 2000*, A.v.d. Berg, W. Olthuis, and P. Bergveld, Editors. 2000, Kluwer Academic Publishers: Dordrecht, The Netherlands. p. 249-252.

48. Fujii, T., *PDMS-Based Microfluidic Devices for Biomedical Applications.* Microelectronic Engineering, 2002. **61-62**: p. 907-914.

49. Hosokawa, K., T. Fujii, and I. Endo. *Hydrophobic microcapillary vent for pneumatic manipulation of liquid in µTAS*. in *MicroTotal Analysis Systems '98*. 1998. Banff, Canada: Kluwer Acad.

50. Lippert, T., *Laser Application of Polymers* in *Polymers and Light*. 2004, Springer Berlin: Heidelberg, Germany. p. 51-246.

51. Roberts, M.A., et al., *UV Laser Machined Polymer Substrates for the Development of Microdiagnostic Systems* Analytical Chemistry, 1997. **69**(11): p. 2035-2042.

52. Ford, S.M., et al., *Microcapillary Electrophoresis Devices Fabricated Using Polymeric Substrates and X-Ray Lithography.* Journal of Microcolumn Separations, 1998. **10**(5): p. 413-422.

53. Lee, L.P., et al. *Key Elements of a Transparent Teflon Microfluidic System*. in *MicroTotal Analysis Systems '98*. 1998. Banff, Canada.

54. Rossier, J.S., et al. *Polymer Microstructures: Prototyping, Low-Cost Mass Fabrication and Analytical Applications*. in *MicroTotal Analysis Systems 2000*. 2000.

55. Backhouse, C., et al., *DNA Sequencing in a Monolithic Microchannel Device.* Electrophoresis, 2000. **21**: p. 150-156.

56. Kaigala, G.V., et al., *Rapid Prototyping of Microfluidic Devices With a Wax Printer.* Lab on a Chip, 2007. **7**: p. 384-387.

57. Xia, Y. and G.M. Whitesides, *Soft Lithography.* Annual Review of Materials Science, 1998 - Annual Reviews, 1998. **28**: p. 153-184.

58. Ye, M.-Y., X.-F. Yin, and Z.-L. Fang, *DNA Separation With Low-viscosity Sieving Matrix on Microfabricated Polycarbonate Microfluidic Chips.* Analytical and Bioanalytical Chemistry, 2005. **381**(4): p. 820-827.

59. Rossier, J.S., R. Ferrigno, and H.H. Girault, *Electrophoresis With Electrochemical Detection in a Polymer Microdevice.* Journal of Electroanalytical Chemistry, 2000. **492**(1): p. 15-22.

60. Ito, T., et al., *Fabrication of Microstructure Using Fluorinated Polyimide and Silicone-based Positive Photoresist.* Microsystem Technologies, 2000. **6**(5): p. 165-168.

61. Smela, E., *Microfabrication of PPy Microactuators and Other Conjugated Polymer Devices* Journal of Micromechanics and Microengineering, 1999. **9**(1): p. 1-18.

62. Lee, G.-B., et al., *Microfabricated Plastic Chips by Hot Embossing Methods and Their Applications for DNA Separation and Detection* Sensors and Actuators B: Chemical, 2001. **75**(1-2): p. 142-148.

63. Abgrall, P., L.-N. Low, and N.-T. Nguyen, *Fabrication of Planar Nanofluidic Channels in a Thermoplastic by Hot-embossing and Thermal Bonding.* Lab on a Chip, 2007. **7**(4): p. 520-522.

64. Kroschwitz, J.I., *High Performance Polymers and Composites*. 1991: John Wiley & Sons, Inc.

65. Aumiller, G.D., et al., *Submicrometer Resolution Replication of Relief Patterns for Integrated Optics.* Journal of Applied Physics, 1974. **45**(10): p. 4557-4562.

66. Masuda, S., M. Washizu, and T. Nanba, *Novel Method of Cell Fusion in Field Constriction Area in Fluid Integrated Circuit.* IEEE Transactions on Industry Applications, 1989. **25**(4): p. 732-737.

67. Toepke, M.W. and D.J. Beebe, *PDMS Absorption of Small Molecules and Consequences in Microfluidic Applications.* Lab on a Chip, 2006. **6**(12): p. 1484-1486.

68. Lee, J.N., C. Park, and G.M. Whitesides, *Solvent Compatibility of Poly(dimethylsiloxane)-Based Microfluidic Devices.* Analytical Chemistry, 2003. **75**(23): p. 6544-6554.

69. Heo, Y.S., et al., *Characterization and Resolution of Evaporation-Mediated Osmolality Shifts That Constrain Microfluidic Cell Culture in Poly(dimethylsiloxane) Devices.* Analytical Chemistry, 2007. **79**(3): p. 1126-1134.

70. Eddington, D.T., J.P. Puccinelli, and D.J. Beebe, *Extended Curing and Reduced Hydrophobic Recovery of Polydimethylsiloxane.* Sensors and Actuators B: Chemical, 2006. **114**: p. 170-172.

71. Bayer, H. and H. Engelhardt, *Capillary Electrophoresis in Organic Polymer Capillaries.* Journal of Microcolumn Separations, 1996. **8**(7): p. 479-484.

72. Piruska, A., et al., *The Autofluorescence of Plastic Materials and Chips Measured Under Laser Irradiation.* Lab on a Chip, 2005. **5**(12): p. 1348-1354.

73. Ku, H.Y. and L.C. Scala, *Polymeric Electron Beam Resist.* Journal of The Electrochemical Society, 1969. **116**(7): p. 980-985.

74. Nagai, N., T. Matsunobe, and T. Imai, *Infrared Analysis of Depth Profiles in UV-photochemical Degradation Polymers.* Polymer Degradation and Stability, 2005. **88**(2): p. 224-233.

75. Khanarian, G. and H. Celanese, *Optical Properties of Cyclic Olefin Copolimers.* Optical Engineering, 2001. **40**(6): p. 1024-1029.

76. *CRC Handbook of Chemistry and Physics*. 87 ed, ed. D.R. Lide. 2007, Boca Raton, Florida: Taylor and Francis.

77. Keddie, J.L., R.A.L. Jones, and R.A. Cory, *Interface and Surface Effects on the Glass-transition Temperature in Thin Polymer-films.* Faraday Discussions, 1994. **98**: p. 219-230.

78. Fryer, D.S., et al., *Dependence of the Glass Transition Temperature of Polymer Films on Interfacial Energy and Thickness.* Macromolecules, 2001. **35**(16): p. 5627-5634.

79. Mukhopadhyay, R., *When PDMS Isn't the Best.* Analytical Chemistry, 2007. **79**(9): p. 3248-3253.

80. Bacher, W., et al., *Fabrication of LIGA Mold Inserts* Microsystem Technologies, 1997. **4**(3): p. 117-119.

81. Grzybowski, B.A., et al., *Generation of Micrometer-Sized Patterns for Microanalytical Applications Using a Laser Direct-Write Method and Microcontact Printing.* Analytical Chemistry, 1998. **70**(22): p. 4645-4652.

82. Heckele, M., W. Bacher, and K.D. Muller, *Hot Embossing - The molding Technique for Plastic Microstructures.* Microsystem Technologies, 1998. **4**: p. 122-124.

83. Becker, H. and U. Heim, *Hot Embossing as a Method for the Fabrication of Polymer High Aspect Ratio Structures.* Sensors and Actuators A, Physical, 2000. **83**(1-3): p. 130-135.

84. Lehr, H. and W. Ehrfeld, *Advanced Microstructure Products by Synchrotron Radiation Lithography.* Journal de Physique IV, 1994. **4**(9): p. 229-236.

85. Henzi, P., et al., *Modification of Polymethylmethacrylate by Deep Ultraviolet Radiation and Bromination for Photonic Applications.* Journal of Vacuum Science and Technology B, 2006. **24**(4): p. 1755-1761.

86. Greeneich, J.S., *Solubility Rate of Poly-(Methyl Methacrylate), PMMA, Electron-Resist.* Journal of The Electrochemical Society, 1974. **121**(12): p. 1669-1671.

87. Dobisz, E.A., et al., *Effects of Molecular Properties on Nanolithography in Polymethyl Methacrylate.* Journal of Vacuum Science and Technology B, 2000. **18**(1): p. 107-111.

88. Greeneich, J.S., *Developer Characteristics of Poly-(Methyl Methacrylate) Electron Resist.* Journal of The Electrochemical Society, 1975. **122**(7): p. 970-976.

89. Greeneich, J.S., *Time Evolution of Developed Contours in Poly-(Methyl Methacrylate) Electron Resist.* Journal of Applied Physics, 1974. **45**(12).

90. Johnstone, R.W., *Self-sacrificial Surface-micromachining Using Poly(methyl methacrylate).* Ph.D. Thesis, 2008.

91. Hiraoka, H., *Radiation-Chemistry of Poly(methacrylates).* IBM Journal of Research and Development, 1977. **21**(2): p. 121-130.

92. Kudoh, H., et al., *Low temperature gamma-ray irradiation effects on polymer materials .3. gas evolution and change of molecular weight.* Radiation Physics and Chemistry, 1996. **48**(1): p. 95-100.

93. Guckel, H., et al. *Deep x-Ray and UV Lithographies for Micromechanics*. in *Solid-State Sensor and Actuator Workshop*. 1990.

94. Meyer, P., A. El-Kholi, and J. Schulz, *Investigations of the Development Rate of Irradiated PMMA Microstructures in Deep X-Ray Lithography.* Microelectronic Engineering, 2002. **63**(4): p. 319-328.

95. Bolorizadeh, M. and D.C. Joy, *Low Voltage Electron Beam Lithography in PMMA*, in *Technical Proceedings of the 2004 NSTI Nanotechnology Conference and Trade Show*. 2005. p. 267-270.

96. Hu, W., et al., *Low Temperature Development of PMMA For Sub-10-nm Electron Beam Lithography*, in *Third IEEE Conference on Nanotechnology, 2003. IEEE-NANO*. 2003: San Francisco, CA, USA. p. 602-605.

97. Mahabadi, K.A., et al., *Fabrication of PMMA Micro- and Nanofluidic Channels by Proton Beam Writing: Electrokinetic and Morphological Characterization.* Journal of Micromechanics and Microengineering, 2006. **16**(7): p. 1173-1180.

98. Breese, M.B.H., et al., *Mev Ion Beam Lithography of PMMA.* Nuclear Instruments and Methods in Physics Research B, 1993. **77**(1-4): p. 169-174.

99. Gonin, Y., et al., *Creating Sub-Surface Channels in PMMA with Ion Beam Lithography in Only One Step.* Applied Surface Science, 2003. **217**(1-4): p. 289-293.

100. Burke, B.G., et al., *Deep-UV Pattern Definition in PMMA.* Nanotechnology, 2008. **19**(21): p. 5301- 5307.

101. Lin, B.J., *Deep-UV Lithography.* Journal of Vacuum Science and Technology 1975. **12**(6): p. 1317-1320.

102. Uhl, A., et al., *DUV and E-Beam Chemistry of High-Sensitivity Positive PMMA-Based Resist*, in *Procedeengs of the SPIE*. 1999.

103. Moore, J.A. and J.O. Choi, *Degradation of Poly(methyl methacrylate): Deep UV, X-ray, Electron-beam, and Proton-beam Irradiation.* ACS Symposium Series, 1991. **475**: p. 156-192.

104. Vladimirsky, Y., et al., *PMMA as an X-ray Resist for Micro-machining Application: Latent Image Formation and Thickness Losses.* Microelectronic Engineering, 1996. **30**(1): p. 543-546.

105. Kawamura, Y., K. Yoyoda, and S. Namba, *Effective Deep Ultraviolet Photoetching of Polymethyl Methacrylate by an Excimer Laser.* Applied Physics Letters, 1982. **40**(5): p. 374-375.

106. Kawamura, Y., K. Yoyoda, and S. Namba, *Deep UV Submicron Lithography by Using a Pulsed High-power Excimer Laser.* Journal of Applied Physics, 1982. **53**(9): p. 6489-6490.

107. Jain, K., C.G. Willson, and B.J. Lin, *Ultrafast High-resolution Contact Lithography with Excimer Lasers.* IBM Journal of Research and Development, 1982. **26**(2): p. 151-159.

108. Estler, R.C. and N.S. Nogar, *Mass Spectroscopic Identification of Wavelength Dependent UV Laser Photoablation Fragments From Polymethylmethacrylate.* Applied Physics Letters, 1986. **49**(18): p. 1175-1177.

109. Küper, S., S. Modaressi, and M. Stuke, *Photofragmentation Pathways of a PMMA Model Compound Under UV Excimer Laser Ablation Conditions.* Journal of Physical Chemistry, 1990. **94**(19): p. 7514-7518.

110. Choi, J.O., et al., *Degradation of Poly(methylmethacrylate) by Deep Ultraviolet, X-Ray, Electron Beam, and Proton Beam Irradiations.* Journal of Vacuum Science and Technology B, 1988. **6**(6): p. 2286-2289.

111. Mimura, Y., et al., *Deep-UV Photolithorgaphy* Japanese Journal of Applied Physics, 1978. **17**(3): p. 541-550.

112. Achenbach, S., et al., *Fabrication of RF Variable capacitors by Deep X-ray Lithography and Electroplating.* Microsystem Technologies, 2006. **13**(3-4): p. 343-347.

113. Becker, E.W., et al., *Fabrication of Microstructures with High Aspect Ratios and Great Structural Heights by Synchroton Radiation Lithography, Galvanoforming, and Plastic Moulding (LIGA Process)* Microelectronic Engineering, 1986. **4**(1): p. 35-36.

114. Ehrfeld, W. and H. Lehr, *Deep X-ray-lithography for the Production of 3-dimensional microstructures from Metals, Polymers, and ceramics.* Radiation Physics and Chemistry, 1995. **45**(3): p. 349-365.

115. Ehrfeld, W. and D. Münchmeyer, *Three-dimensional Microfabrication Using Synchrotron Radiation.* Nuclear Instruments and Methods in Physics Research A, 1991. **303**(3): p. 523-531.

116. Harris, R.A., *Polymethyl Methacrylate as an Electron Sensitive Resist.* Journal of The Electrochemical Society, 1973. **120**(2): p. 270-274.

117. Mohsin, M.A. and M.G. Cowie, *Enhanced Sensitivity in the Electron Beam Resist Poly(methyl methacrylate) Using Improved Solvent Developer.* Polymer, 1988. **29**(12): p. 2130-2135.

118. Bernstein, G.H., D.A. Hill, and W.P. Liu, *New High-contrast Developers for Poly(methyl methacrylate) Resist.* Applied Physics Letters, 1992. **71**(8): p. 4066-4075.

119. Beaumont, S.P., et al., *Sub-20-nm-wide Metal Lines by Electron-beam Exposure of Thin Poly(methyl methacrylate) Films and Liftoff.* Applied Physics Letters, 1981. **38**(6): p. 436-439.

120. Hall, T.M., A. Wagner, and L.F. Thompson, *Ion Beam Exposure Characteristics of Resists.* Journal of Vacuum Science and Technology, 1979. **16**(6): p. 1889-1892.

121. Teh, W.H., et al., *Cross-linked PMMA as a Low-dimensional Dielectric Sacrificail Layer.* Journal of Microelectromechanical Systems, 2003. **12**(5): p. 641-648.

122. Vieu, C., et al., *Electron Beam Lithography: Resoultion Limits and Applications.* Applied Surface Science, 2000. **164**: p. 111-117.

123. Olzierski, A. and I. Raptis, *Development and Molecular-weight Issues on the Lithographic Performance of Poly(methyl methacrylate).* Microelectronic Engineering, 2004. **73-74**: p. 244-251.

124. Flanders, D.C., *Replication of 175-å Lines and Spaces in Polymethylmetacrylate Using X-ray Lithography.* Applied Physics Letters, 1980. **36**(1): p. 93-96.

125. Smith, B.W., T.D. Eakin, and D.W. Johnson. *Characterization of Safe Solvent PMMA Resist variables for Electron-beam Application*. in *Proceedings of SPIE*. 1994.

126. Pethrick, R.A. and K.E. Rankin, *Quantitative Investigation of Factors Influencing the Efficiency of Development of Electron Beam Resists.* Microelectronic Engineering, 1995. **26**(3-4): p. 141-153.

127. Hang, Q., D.A. Hill, and G.H. Bernstein, *Efficient Removers for Poly(methyl methacrylate)* Journal of Vacuum Science and Technology B, 2003. **21**(1): p. 91-97.

128. Pethrick, R.A. and K.E. Rankin, *Influence of Molar Mass on the Diffusion and Solubility Behaviour of Methyl Ethyl Ketone - Isopropil Alcohol Mixtures in Poly(methyl methacrylate).* Journal of Materials Chemistry, 1998. **8**(12): p. 2599-2603.

129. Yasin, S., M.N. Khalid, and D.G. Hasko, *Reduction in Roughness of Resist Features in PMMA Due to the Absence of a Rinse.* Japanese Journal of Applied Physics, 2004. **43**(10): p. 6984-6987.

130. Rooks, M.J., et al., *Low Stress Development of Poly(methyl methacrylate) for High Aspect Ratio Structures.* Journal of Vacuum Science and Technology B, 2002. **20**(6): p. 2937-2941.

131. Patenburg, F.J., S. Achenback, and J. Mohr, *Influence of Developer Temperature and Resist Material on the Structure Quality in Deep X-ray Lithography.* Journal of Vacuum Science and Technology B, 1998. **16**(6): p. 3547-3551.

132. Tan, M.X., et al., *Pmma Development Studies Using Various Synchroton Sources and Exposure Conditions.* Proceedings of SPIE, 1998. **3512**: p. 262-270.

133. Yasin, S., D.G. Hasko, and H. Ahmed, *Comparison of MIBK/IPA and Water/IPA as PMMA Developers for Electron Beam Nanolithography.* Microelectronic Engineering, 2002. **61-62**: p. 745-753.

134. Cowie, J.M.G., M.A. Mohsin, and I.J. McEwen, *Alcohol-water Cosolvent Systems for Poly(methyl methacrylate).* Polymer, 1987. **28**(9): p. 1569-1572.

135. Yasin, S., D.G. Hasko, and H. Ahmed, *Fabrication of <5 nm Width Lines in Poly(methylmethacrylate) Resist Using a Water:Isopropil Alcohol Developer and Ultrasonically-assisted Development.* Applied Physics Letters, 2001. **78**(18): p. 2760-2762.

136. Lavaleé, E., J. Beauvais, and J. Beerens, *electron Beam Lithography of Nanostructures Using 2-propanol:Water and 2-propanol:Methyl isobutyl Ketone as Developers for Polumethylmethacrylate.* Journal of Vacuum Science and Technology B, 1998. **16**(3): p. 1255-1257.

137. Patenburg, F.J., S. Achenbach, and J. Mohr, *Characterization of Defects in Very High Deep-etch X-ray Lithography microstructures.* Microsystem Technologies, 1998. **4**(2): p. 89-93.

138. Hasko, D.G., S. Yasin, and A. Mumtaz, *Influence of Developer and Development Conditions on the Behavior of High Molecular Weight Electron Beam Resists.* Journal of Vacuum Science and Technology B, 2000. **18**(6): p. 3441-3444.

139. Lee, K.L., et al., *Ultrasonic and Dip Resist Development Processes for 50 nm Device Fabrication.* Journal of Vacuum Science and Technology B, 1997. **15**(6): p. 2621-2626.

140. *Optix® Acrylic Sheet.* www.plaskolite.com/productguide/04.pdf.

141. Tao, S.L. and T.A. Desai, *Microfabrication of Multilayer, Asymmetric, Polymeric Devices for Drug Delivery.* Advanced Materials, 2005. **17**(13): p. 1625-1630.

142. Mendonca, C.R., et al., *Femtosecond Laser Waveguide Micromachining of PMMA Films with Azoaromatic Chromophores.* Optics Express,, 2008. **16**(1): p. 200-2006.

143. *GoodFellow CQ Acrylic Sheet ME303031.* https://www.goodfellow.com/home.aspx?LangType=1033.

144. *CYRO Acrylite® OP-4 Acrylic Sheet.* http://www.sdplastics.com/acryliteliterature/1354BOP4UVtransTECHDATA.pdf.

145. Charlesby, A., *Polymethyl Methacrylate*, in *Atomic Radiation and Polymers*, P. Press, Editor. 1960: New York.

146. Kelen, T., *Photodegradation*, in *Polymer Degradation*. 1982, Van Nostrand Reinhold: New York.

147. Li, J.H., D. Chen, and G. Chen, *Low-Temperature Thermal Bonding of PMMA Microfluidic Chips.* Analytical Letters, 2005. **38**(7): p. 1127-1136.

148. Sun, Y., Y.C. Kwok, and N.T. Nguyen, *Low-Pressure, High-Temperature Thermal Bonding of Polymeric Microfluidic Devices and Their Applications for Electrophoretic Separation.* Journal of Micromechanics and Microengineering, 2006. **16**(8): p. 1681-1688.

149. Gupta, A., et al., *Characterization of a Dissociative Excited State in the Solid State: Photochemistry of Poly(methy1 methacrylate). Photochemical Processes in Polymeric Systems.* Macromolecules, 1980. **1980**(13): p. 1696-1700.

150. Bligh, M., et al., *Two-Phase Interdigitated Microelectrode Arrays for Electrokinetic Transport of Microparticles.* Journal of Micromechanics and Microengineering, 2008. **18**(5): p. 55007-550016.

151. Wu, S., *Polymer Interface and Adhesion*. 1982: CRC Press. 630.

152. Kruse, A., et al., *Surface Pretreatment of Plastics for Adhesive Bonding.* Journal of Adhesion Science and Technology, 1995. **9**(12): p. 1611-1621.

153. Shenton, M.J., M.C. Lovell-Hoare, and G.C. Stevens, *Adhesion Enhancement of Polymer Surfaces by Atmospheric Plasma Treatment.* Journal of Physics D: Applied Physics, 2001. **34**: p. 2754-2760.

154. Hu, S. and W.J. Brittain, *Surface Grafting on Polymer Surface Using Physisorbed Free Radical Initiators.* Macromolecules, 2005. **38**(15): p. 6592-6597.

155. Uyama, Y., K. Kato, and Y. Ikada, *Surface Modification of Polymers by Grafting* Advances in Polymer Science, 1998. **137**: p. 1-39.